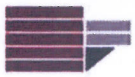

UNIVERSITY OF CALABRIA

DOCTORAL DISSERTATION

SSD: ICAR/08 SCIENZA DELLE COSTRUZIONI

Numerical tools for moisture-stress and fracture analysis of timber structures

Author:
Antonio Lorenzo MENDICINO

Supervisors:
Dr. Antonio BILOTTA
Dr. Stefania FORTINO

Coordinator:
Prof. Maurizio ARISTODEMO

November 25, 2010

Abstract

This work presents numerical tools for the evaluation of moisture induced stresses in timber structures and for the analysis of cracked glulam structures. The work is related to the European WoodWisdom-Net project Improved Moisture and the Cost Action E55 project, which are gratefully acknowledged.

A multi-Fickian approach for the moisture transfer modelling is used. A moisture-stress analysis based on a 3D orthotropic-viscoelastic-mechanosorptive model for wood is performed by using the Abaqus FEM code. The constitutive model and the needed equations of moisture diffusion are implemented into some Abaqus user subroutines. The results, in terms of moisture content and stress, are compared with experimental data available in the literature. The numerical values of moisture content and stresses are found to be in good agreement with the experimental data. This is promising for the development and the extension of the method to more general cases of timber connections under natural humidity conditions. For more general cases, the use of a multi- Fickian analysis would require future computational work aimed to implement a hysteresis model suitable to describe real humidity conditions as suggested in (Frandsen 2007).

The moisture-stress analysis method implemented can also be further developed for the analysis of cracked timber structures (Zagari et al. 2009). This topic is important because, under service conditions of buildings, the moisture induced stresses can influence the durability of timber structures by inducing crack propagation (Vasic & Stanzl-Tschegg 2007, Sjödin 2008).

The crack growth simulation under short-term loading is done by using a suitable exponential damage law and the cohesive elements of Abaqus in the fracture process zone. The optimal parameters for the damage law are determined through a parametric study involving a certain number of nonlinear analyses for monotonically proportional loads scaled with respect to the experimental fracture energy of the specimen. The proposed computational approach is validated by analyzing glued laminated (glulam) specimens under opening mode and the numerical load-displacement curves are compared with both literature results and experimental data obtained in the context of the present research. For long-term fracture tests under sustained loads and constant moisture content, a criterion of crack initiation based on a viscoelastic integral parameter is also introduced. The computational approach can be further extended to cases of crack propagation in the presence of variable humidity conditions.

Abstract

La tesi presenta alcuni strumenti numerici per la valutazione delle tensioni provocate dall'umidità nelle strutture in legno e per la modellazione dei fenomeni di frattura nelle strutture in legno lamellare incollato. Il lavoro è stato svolto in collegamento con lo European WoodWisdom-Net project Improved Moisture e il Cost Action E55 project. A tal proposito si ringraziano gli staff di tali programmi di ricerca.

Sono state condotte analisi tensioni-umidità basate su un modello 3D ortotropo-viscoelastico-mechanosorptive per il legno e su un modello multi-Fickian per la diffusione dell'umidità. Il modello complessivo è stato implementato nel codice FEM Abaqus: in particolare il modello costitutivo del materiale solido, il flusso esterno di umidità e il sorption per unità di tempo sono stati implementati tramite l'intefaccia Abaqus delle user subroutine. I risultati in termini di umidità e tensioni sono stati confrontati con dati sperimentali disponibili in letteratura. I valori numerici ottenuti risultano essere sufficientemente in accordo con i dati sperimentali. Perciò il modello potrebbe essere ulteriormente sviluppato ed esteso ai casi più generali dei collegamenti per le strutture in legno in condizioni reali di umidità. Per i casi più generali, l'uso dell'analisi multi-Fickian analysis richiederebbe l'implementazione di un modello di isteresi, suggerito in letteratura come adatto a descrivere condizioni climatiche naturali.

Il metodo di analisi tensioni-umidità potrebbe essere inoltre ulteriormente sviluppato per l'analisi di strutture in legno soggette a frattura. Tali argomenti risultano molto importanti allo stato attuale, poiché, in condizioni di servizio, le tensioni provocate dall'umidità, provocando la propagazione delle fratture, possono influenzare la durabilità delle strutture in legno.

Nel lavoro di tesi, la simulazione della crescita delle fratture in condizioni di carico short-term è stata fatta utilizzando una legge di danno esponenziale e gli elementi coesivi del codice FEM Abaqus. I valori ottimali dei parametri della legge di danno sono stati determinati attraverso uno studio parametrico condotto lanciando un certo numero di analisi non lineari con carichi monotoni. L'approccio computazionale proposto è stato validato analizzando provini in legno lamellare incollato soggetti al modo I di frattura e le curve numeriche carico-spostamento sono state confrontate con dati sperimentali ottenuti nell'ambito del progetto Improved Moisture. Per i test di frattura long-term in condizioni di carichi fissi e contenuto d'acqua costante, un criterio di frattura basato su di un parametro integrale viscoelastico è stato inoltre introdotto.

L'approccio computazionale potrebbe essere esteso a casi di propagazione della frattura in presenza di umidità variabile.

Contents

Preface

This thesis presents numerical tools for 3D moisture-stress and fracture analysis for timber structures under variable humidity and load conditions.
The document has a usual organization which is the following:

- In chapter 1, an introduction to the subject is given .
- In chapter 2, a discussion about the background on the subject is given.
- In chapter 3, the methods used in the tools studied are discussed.
- In chapter 4, the algorithm followed in the implementation .
- In chapter 5, the implementation realized is described .
- In chapter 6, some results of the work are presented.
- In chapter 7, some conclusions are provided.
- In appendix chapter A, list of symbols used in this report is given.
- In appendix chapter B, input files listing is given.

Chapter 1

Introduction

1.1 Moisture-stress analysis

The mechanical response of wood in presence of moisture changes is a fundamental topic for both the serviceability and the safety of timber structures (**???**). It is assumed that stresses in the plane perpendicular to the grain direction affect the strength of glulam beams during variable environmental conditions (**??**). Also the strength of timber connections in the cross grain direction is influenced by moisture induced deformations (**?**). In general, the combination of moisture history and mechanical loading is important under service conditions, that is under relative low loads and natural temperatures and humidities (**?**). According to **?**, in this context the moisture effect can be considered as an action to be combined with the external mechanical loads. The failure modes in wood and the crack growth under both constant and varying humidity levels in timber structures are challenging research topics as well (**???**).

In the last two decades, several material models based on experiments under different mechanical loads and humidity conditions were proposed (see references in **??**). These models take into account the interaction between varying moisture and stress, called mechanosorption or mechanosorptive creep, and sometimes neglect the effect of the viscoelastic creep, which is normally found at constant moisture contents. **?** proposed a general 3D mathematical formulation for creep of orthotropic wood in drying conditions where the coupling between viscoelastic and mechanosorptive creep was taken into account. However, only a 2D mechanical analysis of wood in the section perpendicular to grain was performed. In fact, since wood is a variable, heterogeneous and anisotropic material, the identification of creep parameters for 3D models is a very difficult task. In spite of the available experimental data on the viscoelastic creep and the mechanosorptive effect in timber structures in grain or in cross grain direction, there is still a lack of both experimental work and theoretical background, for example about the Poisson ratios to be used in 3D wood material models in the presence of viscoelastic effects and moisture gradients. Recent advances on

this subject were presented by **?**. On the other hand, for the efficient design of timber structures, the formulation of a reliable 3D model for wood is important and the finite element code Abaqus represents a suitable computational tool for implementing constitutive models and for the simulation of three–dimensional coupled problems in engineering (**?**). Recent literature shows a growing interest in modelling 3D orthotropic wood structures by Abaqus (**???**). Also 3D fracture mechanics problems in wood can be solved, at least in the elastic case, by using the cited code (see **??**).

This work presents a 3D coupled moisture-stress numerical analysis for timber structures designed to be used in service conditions of buildings. The analysis is based on a constitutive orthotropic viscoelastic-mechanosorptive model. The rheological model is characterized by five deformation mechanisms and, as proposed by **?**, a thermodynamic formulation is used starting from the Helmholtz free energy expressed as a function of temperature, moisture content, total strain, viscoelastic strain and recoverable mechanosorptive strain. The used viscoelastic model is an extension of the 1D formulation proposed by **?** for parallel to grain direction and consists of a sum of Kelvin type elemental deformations. The mechanosorptive model contains an irrecoverable part plus a series of Kelvin elements and is a combination of the 1D model introduced by **?** for cross grain direction and of the 1D model for longitudinal direction of wood presented by **?**. The extension of the previous models to 3D is based on three–dimensional elemental viscoelastic and mechanosorptive matrices. In this work, temperature is considered to be constant. The temperature effect was not found of relative significance on the deformation behaviour, at least in the natural temperature ranges (**?**).

The viscoelastic-mechanosorptive constitutive model is implemented in the user subroutine UMAT of the FEM code Abaqus (**?**). The algorithm for moisture induced stress update, based on the concept of algorithmic tangent operator (**?**), is a variant of the one proposed by **?**. Furthermore, the equations needed to describe the moisture flow across the structure are implemented into the Abaqus user subroutine DFLUX. Using the analogy with the temperature–displacement analysis available in the Abaqus/Standard code, a coupled moisture-stress analysis is performed under different mechanical loads and moisture changes. The analysis is validated by analyzing some of the tests carried out by **?**, **??** and **?** and by comparing the computational results with the reported experimental data. These comparisons are an important aspect of the present paper. In this work, particular emphasis is posed on the general and flexible 3D computational tool which permits to successfully solve coupled moisture-stress analyses of timber structures under different types of loads and environmental conditions.

1.2 Fracture analysis

The mechanical response of wood under sustained loads and variable moisture conditions is an important topic for the durability and safety of glued laminated timber (glulam) [1,2,3]. Both the viscoelastic creep and the used adhesives can

affect the crack propagation in glulam structures. Despite the importance of this subject, relatively few scientific publications are available on the viscoelastic creep crack growth in wood [4] and on the fracture parameters of glue-lines in glued wooden products [5]. For both solid wood and wooden glue-lines there is a lack of specimens suitable to study crack propagation at sustained loads with eventual impact of moisture variations [6,7,8,9]. In the present paper the three-dimensional orthotropic-viscoelastic model introduced by Fortino et al. in [10] is used. The rheological scheme is based on elastic strains and Kelvin type elemental deformations which are described by using an extension to 3D of previous 1D and 2D models for wood in the grain direction and in the perpendicular to grain direction [11,12]. The 3D compliance viscoelastic matrix of the model is assumed to be proportional to the elastic compliance matrix in the reference conditions of temperature and moisture content. A thermodynamic formulation is used starting from the Helmholtz free energy as proposed by Hanhijärvi and Mackenzie-Helnwein in [12]. The stress increment at the new time step is calculated on the basis of the total tangent operator of the model as done in [13]. The constitutive model and the algorithm for stress update are implemented into the Umat subroutine of Abaqus FEM code [14]. In this work the phenomenon of crack propagation for both short-term and long-term problems is studied. In the short-term case, the load-displacement curve under constant humidity conditions of the specimen subjected to fracture test plays a fundamental role in the determination of the fracture energy of the specimen. In fact the fracture energy can be directly determined from the area under the curve in the case of stable crack propagation. To perform an accurate computational approach for short-term cases, the Stanzl et al. wedge- splitting specimen under opening mode is analyzed [15]. Since for this test the direction of crack propagation is known, the fracture process zone (FPZ) can be described by using the cohesive elements of Abaqus and a suitable exponential damage law defined on the basis of load- displacement curves of the analyzed cracked specimen. The parameters characterizing the damage curve are obtained through a parametric study performed by using several nonlinear analyses solved by the Riks method of Abaqus/Standard and some Script tools as proposed in [16]. The wedge-splitting specimen is analyzed in both the radial-longitudinal (RL) and the tangential- longitudinal (TL) crack configurations of wood. During the nonlinear analysis for short-term tests the viscoelastic effects are assumed to be negligible. The method is validated by comparing the numerical load- displacement curve of a modified DCB glulam specimen under opening mode with experimental data carried out in the context of the present research. The specimen lamellas are glued with a polyurethane adhesive and the crack is forced to propagate at the interface between lamellas. In this case, the load-displacement curve furnishes the fracture energy of the interface. The method is also suitable for the analysis of cracked specimen under Mode II short-term loading with crack propagation along the glue-lines. For the long-term case, a generalized version of the well- known J integral parameter is defined, which includes the viscoelastic strain characterizing the proposed constitutive model. In this case, a modified PTENF specimen under Mode II loading is analyzed since it shows more stable

crack growth behaviour with respect to the Mode I DCB specimens. After fixing a critical value of J integral, corresponding to the experimental fracture energy obtained with the short-term test, the specimen is loaded by a constant load corresponding to 80in short-term tests. The reduced sustained load will cause crack initiation at a certain critical time. The introduction of a viscoelastic J integral and the concept of critical time permit to define a criterion of crack initiation during time for wood structures under sustained loads in the presence of constant moisture content. To develop crack propagation criteria in the presence of variable humidity conditions further theoretical work is needed (see [17,18]).

Chapter 2

Background

2.1 Moisture transport in wood

Moisture transfer in wood below the fiber saturation point is governed by three phenomena:

- bound-water diffusion
- water-vapor diffusion
- phase change or sorption, which contributes to the previous equations with the term $\dot{c}$, i.e. the phase change per unit of time.

2.1.1 Taking moisture in wood into account

From a design point of view the Eurocode 5 (CEN 2004) currently considers the effect of moisture on the behaviour of timber structures at Ultimate (ULS) and Serviceability (SLS) Limit State through the coefficients k_mod and k_def. The influence of the load duration on strength and deflection is accounted for by assigning the structure to a load duration class, which depends on the nature of the load. The higher moisture content and the exposure to severe environment are accounted for by dividing all possible types of environment which the structure may be exposed to in three service classes (1, 2 and 3). This approach is easy to use at the design level as no complex rheological model needs to be used. However, it may be difficult to choose the appropriate service class of a structure. Furthermore, the actual behaviour may differ significantly between small and massive timber structures since in the service class no allowance for the size of the structure is made.

The approach proposed in **?**, in order to simplify the problem, is the following:

- identification of climatic regions within Europe basing on the environmental histories of relative humidity RH=RH(t) for a period of ten years.

- selection of a number of timber cross-section of technical interest: narrow (sawn timber, 38x225 mm), medium (glulam, 115x240 mm), cross-lam (2400x150 mm).
- calculate the yearly history of moisture content over the cross-section using the Fick's diffusion laws with particular emphasis on the history of average moisture content for each climatic region and each selected timber cross-section.
- provide tabular values of temperature and moisture content variations due to environmental changes. The values of u=uavg,max-uavg,min and T=Tmax-Tmin could then be provided in codes of practice (for example the Eurocode 5) for the different region and type of cross-section.

2.1.2 Macrostructure characteristic of timber

The characteristic macrostructure of timber is formed by concentric annual rings. These rings are a consequence of the growth increment during each growth season As described in Hanhijärvi (1995), each annual ring is composed of a layer of earlywood which develops rapidly early in the season, and a layer of latewood which develops slowly at the end of the season. Earlywood cell cross section is large and its walls are thin, latewood cell cross-section is smaller and its walls are thicker.

2.1.3 Microstructure characteristic of timber

Almost all species of wood have the same features of wood cells. Elementary fibrils consist of cellulose formed into larger units. Several elementary fibrils together form thread like entries called microfibrils (Blass et al. 1995). Microfibrils contain an estimated number of 100 to 2000 cellulose chains embedded in a matrix of hemicelluloses and enveloped by lignin. Between all individual cells in wood there are a middle lamella (ML) which contains lignin and peptic substances. The most outer layer of the cell is called the primary wall (P). This layer consists of cellulose microfibrils which are arranged in an irregular pattern. After the primary wall there is a secondary wall, this normally consists of three layers S1, S2 and S3 (Figure 2.2). In the very thin first layer (S1) the angle of microfibrils has an average of 50-70°. In the second layer, which is rather thick compared to the other two, the slope of microfibrils is about 5-20°. In tension of fibres this layer is the most important one since most of the tensile force has to be taken by this layer. Closest to the lumen core, layer (S3) has microfibrils with a smaller slope but not in a defined order. In compression the S2 layer will act as a column. To prevent the layer from buckling the S1 and S3 layer act as reinforcement since the microfibrils has a larger slope than the middle layer.

2.1.4 Moisture properties of timber

The wood cells of a living tree are very porous and contain a great deal of water. In fact, the moisture content of wood in a tree can often exceed 100(**?**). Moisture content as defined in all aspects of timber production uses the weight of the moisture in the wood divided by the dry weight of wood material (this is an unusual definition compared with many other materials that use the wet weight as the denominator). In alive trees, there is actually a much bigger mass of water than wood.

Water is stored in wood in two main forms:

- As free water in the vessels and/or cells, used to move nutrients within the tree.
- As cell (or bound) water, which is an integral part of the cell walls.

As soon as the timber is cut, the wood starts to lose moisture. The initial reduction in moisture content is a result of free water loss. This usually occurs without any significant dimensional changes to the timber as the loss of moisture represents the drainage of voids or vessels in the timber. If the environmental conditions are favourable, the moisture loss continues until all the free water is released to the atmosphere. This point is known as the fibre saturation point (FSP). The fibre saturation point varies a little with each piece of timber, but it is generally taken to be at a moisture content of between 25The loss of free water will occur relatively quickly in small cross-sections of timber, even if the timber is exposed to rain. However, in larger cross sections, it can take many decades for all of the free water to be lost. Initial drying of the outside forms a hard "case" which can act as a barrier to further moisture loss. After all of the free water has been lost, the timber will still contain moisture, but this moisture is bound into the cell walls. Much more energy is required to remove this moisture as it is held in the wood structure by weak chemical bonds. This loss of moisture occurs more slowly than the loss of free water. It also results in a reduction in the size of the cell walls, which causes the timber to shrink in size.

Moisture can have a number of detrimental effects on timber:

- Change in cross sectional dimensions - At moisture contents less than fibre saturation point (25drying shrinks. The shrinking and swelling takes place at a range of moisture contents that the wood will experience in normal service.
- Strength - Water in the cell walls tends to make them a little slippery. It acts as a lubricant and allows the fibres to slide past each other a little easier. There is a small reduction in strength of wood fibres as moisture content increases. This effect is seen in the relationship between strength and moisture for clear wood specimens.
- Stiffness - Water lubrication within the cells causes a small increase in elastic deflection under load (this is a decrease in stiffness). However,

moisture has a marked effect on creep. With only loose bonds between the cells, as load is applied, the fibres rely on friction to stop them sliding over each other. Under long term loading, some sliding will occur. This is creep. Water in the cell walls increases the creep markedly by lubricating the slip interface. Creep is accelerated while water is moving into or out of the wood.

- Durability - fungi and termites need to have moisture to thrive. Moist wood is therefore more vulnerable to biological degradation. Most paints and glues are only really effective if applied to dry wood. Moisture therefore can compromise the durability of timber by making conditions more favourable for biological attack and by reducing the effectiveness of protective coatings.

- Coatings - unless the protective coatings are flexible, the shrinkage and swelling of timber as moisture moves in and out causes deterioration of the coatings. Once a coating has been broken, water can move into the timber. The undamaged portion of the coating can trap moisture in the timber. The swelling and shrinkage of the timber in response to changes in moisture content will cause rapid deterioration of the rest of the coating. Paintwork must be kept in good condition, otherwise rapid deterioration of both the paintwork and the timber will result.

2.1.5 Changes in moisture content

Increased moisture content in the cell walls will decrease the mechanical properties of wood. This is due to water penetrating the cell wall which will weaken the hydrogen bonds that hold the cell wall together.

There are different curves depending of the type of wood and temperature of the surrounding air. It takes a long time for wood to adapt its moisture content from the surrounding RH.

2.1.6 Equilibrium moisture content

The actual value of emc is mainly affected by the humidity and temperature of the environment. It can vary a little with the species (but it is only a minor effect).

Since moisture movement under normal moisture gradients is relatively slow, the annual average conditions of humidity and temperature become important. The emc of timber used internally can be affected by the heating or cooling regime for the building. Heating can dry timber more rapidly and depress the emc. Airconditioning also has a major effect on emc as the air is frequently very dry. In order to minimise the movement of moisture into and out of the timber in service, it is good to have the timber close to the equilibrium moisture content when it is installed in the structure. This will reduce any adverse effects of further shrinkage or swelling of the timber in service.

For this reason it is good to store graded products, such as flooring, in the rooms where it is going to be used, for some weeks prior to installation. This allows the timber to reach equilibrium with the environment of the intended use prior to fixing in place.

2.1.7 Rheological phenomena of materials

Some materials of technical interest for structural engineering, like for example concrete and timber, are characterized by a 'rate-dependent' behaviour that means dependent on the speed of load application. In this case materials have a rheological or viscous behaviour, because under constant load they show strains growing in time.

For timber member, whose strain and stress state is influenced by water content, the real rheological behaviour is split into two phenomena. The first viscous phenomenon follows the assumption of not dependence of strain and stresses on the history of water content and temperature. The second mechano-sorptive phenomenon considers the influence of water content variation (Fragiacomo 2001).

2.1.8 Mechano-sorptive phenomenon

The deflection of wood structures in service is practically important, because with the dimensions used, failure usually occurs first by unacceptably large deflections and only at a much later stage by actual rupture. Deflection is partly elastic and partly timedependent creep. Besides the importance of time as variable, it is known that changing humidity causes wood to creep more than at constant humidity, the strain depending only on the amount of moisture change. According to Morlier (1994) following variables are involved in mechano-sorptive creep:

- Wood characteristics
- Time
- Stress
- Stress history
- Moisture content
- Moisture content change
- Moisture content history
- Temperature
- Temperature history

2.1.9 Variation of moisture in timber structures

The timber, if requested by a state of constant tension, has the characteristic to increase significantly its deformation over time due to rheological phenomena. The difficulties in the estimation of the deformation are mainly due to the complex rheological behaviour, since many factors affect the magnitude of deformation deferred. The time, stress, humidity and temperature are also dominant factors. In addition, to measuring the deformation, is not enough in general to consider the above factors, but their history and interaction have to be taken into account. In many studies it was found (Armstrong & Kingston 1962) that a change of humidity within a loaded beam results in additional deformation that can not be predicted by considering separately the responses to the change of humidity and the applied load and their superposition. This effect has been described as "mechano-sorptive" and it determines in condition of variable humidity a deformation greater than the levels that would be achieved by maintaining a constant humidity for each level within the range of variation owner. According to Fragiacomo (2001), rheological behaviour of wood can be described distinguishing between constant moisture behaviour and variable moisture behaviour, which considers the mechano-sorptive phenomenon.

In constant conditions of humidity a generic element of wood under a constant stress state over time shows increasing deformation: this is the phenomenon of viscosity. Unlike concrete, however, the viscous behaviour of wood type is hereditary, that depends only on the duration of load application and not age (Fragiacomo 2001).

In the case of varying conditions of humidity, three effects have to be taken into account (Fragiacomo 2001): a) the variation of elastic modulus of wood with moisture, which produces an elastic deformation in addition to those related to the variation of stress state; b) the mechano-sorptive phenomenon, which produces an increase of deformation deferred; c) the phenomenon of shrinkage / swelling, which produces an additional inelastic deformation.

When a timber member is exposed to the atmosphere, a variation of moisture content $u = u(x, y, z, t)$ will take place over time t in the different points P (x, y, z) of the timber volume. Those variations ??u are governed by the diffusion laws and will depend upon the histories of relative humidity RH=RH(t) and temperature T=T(t) of the environment. Since the moisture content variations ??u are not constant over the cross-section, the corresponding moisture strains will induce eigenstresses and deflections in the timber member (Fragiacomo 2008).

2.2 Fracture in wood

Numerical models for wood fracture and failure are commonly based on the finite element method. Most of these models originate from general theoretical considerations for other materials. This limits their usefulness because no amount of complexity in a model can substitute for lack of an appropriate rep-

resentation of the physical mechanisms involved. As for other materials, wood fracture and failure models always require some degree of experimental calibration, which can introduce ambiguity into numerical predictions because at present there is a high degree of inconsistency in test methods. A literature review of the models for wood fracture in Vasic, 2005.

The main postulate of finite element analysis (FEA) is that complex domains can be discretized and represented by an assembly of simpler finite sized elements. This enables description of the global problem via a system of differential equations that account for inter-element compatibility and boundary conditions requirements. FEA can be used to model a large array of physical situations and processes including problems in the domains of continuum mechanics, heat and mass transfer and fluid flow. The concepts, fundamentals and application of FEA are described in many texts (e.g., Bathe 1996; Cook 1995; Zenkiewicz and Taylor 1988, 1989) . Other numerical techniques are often used to represent solid mechanics problems, e.g., the boundary element method (Aliabadi and Rooke 1993; Brabia 1978), but at this stage at least they are not as fully developed. This paper focuses on stress analysis of fracture problems in wood by FEA methods. The basic premise of modern engineering is that models can be used to extrapolate beyond the range of test data. Therefore, if complex physical processes and phenomena related to fracture in wood are understood for representative situations, numerical models can be built to represent those processes and phenomena beyond the range of those representative situations. FEA and other numerical analysis techniques can therefore never be a total replacement for experimental observations. They are a powerful adjunct that has to be allied with experimental observation and material characterization.

Chapter 3

Methods

All the equations and formulae involved in the algorithms implemented, have been described in this chapter.

All the symbols used in the formulation of the problems are explained in the appendix chapter A.

3.1 Moisture content and moisture induced stresses evaluation

The algorithm implemented for the moisture-stress analysis is based on the multi-Fickian moisture transport model described in Frandsen **?**, **?** and on the visco-elastic mechano-sorptive hygro-mechanical model described in **?**.

3.1.1 Moisture transfer in wood

In the present work, wood material is assumed to follow Fick's law for moisture transfer and the temperature is considered to be constant. As suggested by **?**, the effect of moisture is considered as a further action to be added to the external mechanical loads. For this reason, a coupled moisture-stress analysis seems to be a suitable computational tool for analyzing the moisture induced stresses in wood. Let Ω be the wood domain, Fick's law is expressed as

$$\frac{\partial u}{\partial t}\Big|_{\Omega} = \nabla \cdot (\mathbf{D} \cdot \nabla u) \tag{3.1}$$

where u is the moisture content of wood and $\mathbf{D}$ the second–order diffusion tensor of moisture transfer. Note that this form of the Fick equation can be used when the density of wood ρ is constant. For varying ρ, the variable $c = \rho u$ instead of u has to be considered as the potential (where c represents the concentration in kg/m^3). In literature, the assumption of isotropic diffusion is usually made and only the diagonal coefficients of the matrix form of tensor $\mathbf{D}$ are considered to be nonzero. As pointed out in (**?**), the dependence of the diffusion tensor

on moisture content makes Eq. (3.1) nonlinear but, since the changes of both u and $D(u)$ are small, $D(u)$ may be considered constant during the single time step and a linear solution of Eq. (3.1) can be accepted.

For a more realistic description of diffusion in 3D wood structures, the values of $D(u)$ in the three material directions should be defined. In (**?**), the diffusion coefficients in longitudinal direction D_L and in the transversal direction D_T were calculated for Norway spruce. For the radial direction, $D_R = D_T$ was assumed. In the present work, the following expression of the diffusion coefficient depending on the moisture content is used for wood in radial and tangential direction:

$$D_R(u) = D_T(u) = 8.64 \times 10^{-7} e^{4u} \text{ m}^2\text{h}^{-1} \tag{3.2}$$

This coefficient, based on the expression provided by **?**, is obtained by fitting the experimental results presented in (**?**). In the longitudinal direction, the experimental values of $D_L(u)$ presented by **?** are used. Note that Fick's equation is mathematically analogous to the heat transfer equation:

$$\rho c_T \frac{\partial T}{\partial t}\Big|_\Omega = \nabla \cdot (\boldsymbol{\lambda} \cdot \nabla T) \tag{3.3}$$

where ρ, c_T and T are the density, the specific heat and the temperature of wood, respectively, while $\boldsymbol{\lambda}$ represents the second–order thermal conductivity tensor. The analogy between (3.1) and (3.3) is obtained by posing $c_T = 1$ and $\boldsymbol{\lambda} = \rho\mathbf{D}$. Because of this analogy, the moisture-stress analysis for wood can be performed by using the available temperature-displacement analysis of the Abaqus/Standard code. This code utilizes the UMAT subroutine where the above constitutive model is implemented while the moisture flow equation through the wood surface is implement into the user subroutine DFLUX. The moisture flow at the surface Γ of the wood body is expressed by using the following equation by **?** and **?**:

$$\frac{q_n}{\rho} = S_u(u_{air} - u_{surf}) \tag{3.4}$$

where q_n represents the moisture flow across the boundary, $S_u = 3.2 \times 10^{-8} e^{4u}$ m/s is the coefficient of surface emission (**?**), u_{surf} is the moisture content of the wood surface and u_{air} the equilibrium moisture content of wood corresponding to the air humidity which, according to **?**, may be described with the following function:

$$u_{air} = 0.01 \left(\frac{-(T + 273.15)\ln(1 - h)}{0.13(1 - (T + 273.15)/647.1)^{6.46}} \right)^{1/[110(T+273.15)^{-0.75}]} \tag{3.5}$$

In Eq. (3.4), u_{surf} is the current solution in terms of moisture content, T represents the temperature in Celsius and $h = 0.01 \cdot \%\text{RH}$ where RH is the relative humidity. As pointed out in (**?**), Eq. (3.5) was obtained in (**?**) for the use of the sorption isotherm by **?**.

Moisture transfer is governed by two equations:

- bound-water diffusion equation

$$\frac{\partial}{\partial t}(c_b) + \nabla \bullet (\mathbf{J_b}) = \dot{c} \tag{3.6}$$

- water-vapor diffusion equation

$$\frac{\partial}{\partial t}(c_v) + \nabla \bullet (\mathbf{J_v}) = -\dot{c} \tag{3.7}$$

which, being $c_v = \frac{\varphi M_{H_2O}}{RT} p_v$, can be rewritten as

$$\frac{\varphi M_{H_2O}}{R} \frac{\partial}{\partial t}\left(\frac{p_v}{T}\right) + \nabla \bullet (\mathbf{J_v}) = -\dot{c} \tag{3.8}$$

and for an isothermal case $T = cost(t)$ it is

$$\frac{\varphi M_{H_2O}}{RT} \frac{\partial p_v}{\partial t} + \nabla \bullet (\mathbf{J_v}) = -\dot{c} \tag{3.9}$$

$\dot{c}$ is the coupling term ($\dot{c} = \dot{c}(c_b, p_v)$) among the two equations of the problem and it expresses phase change or sorption, which contributes to the previous equations with the term $\dot{c}$, i.e. the phase change per unit of time.

Diffusion fluxes can be explicited as

$$\mathbf{J_b} = -\mathbf{D_b} \bullet \nabla c_b \tag{3.10}$$

$$\mathbf{J_v} = -\mathbf{D_v} \bullet \nabla \left(p_v \frac{\varphi M_{H_2O}}{RT}\right) \tag{3.11}$$

Using (3.10), equation (3.6) can be rewritten as

$$\frac{\partial c_b}{\partial t} = \nabla \bullet (\mathbf{D_b} \bullet \nabla c_b) + \dot{c} \tag{3.12}$$

Using (3.11), equation (3.9) can be rewritten as

$$\frac{\varphi M_{H_2O}}{RT} \frac{\partial p_v}{\partial t} = \frac{\varphi M_{H_2O}}{RT} \nabla \bullet (\mathbf{D_v} \bullet \nabla p_v) - \dot{c} \tag{3.13}$$

or

$$\varphi \frac{\partial p_v}{\partial t} = \varphi \nabla \bullet (\mathbf{D_v} \bullet \nabla p_v) - \frac{RT}{M_{H_2O}} \dot{c} \tag{3.14}$$

So the problem is composed of two differential equations (3.12, 3.13), one for each diffusing phase, and of two set of boundary conditions, one for each diffusing phase

$$\mathbf{n} \bullet \mathbf{J_v} = k_p (p_v^s - p_v^a) \tag{3.15}$$

$$\mathbf{n} \bullet \mathbf{J_b} = 0 \tag{3.16}$$

A Dirichlet boundary condition instead of the Neumann one (3.15) can be used in case of high air velocity

$$p_v^s = p_v^a, \text{at high air velocity} \tag{3.17}$$

Both bound water and water vapor diffusivities are described by two coefficients (orthotropy): the bigger one is that for longitudinal direction, the other is for transversal directions.
Bound water diffusivity, $\mathbf{D_b}$, can be calculated as

$$\mathbf{D_b} = \begin{bmatrix} D_b^L & 0.0 \\ 0.0 & D_b^T \end{bmatrix} \exp\left(\frac{-E_b}{RT}\right) \tag{3.18}$$

where

$$E_b = (38.5 - 29m) \times 10^3 Jmol^{-1} \tag{3.19}$$

Vapor diffusivity, $\mathbf{D_v}$, can be calculated as

$$\mathbf{D_v} = \begin{bmatrix} \xi_L & 0.0 \\ 0.0 & \xi_T \end{bmatrix} D_v^0 \left(\frac{p_{atm}}{p_{atm} + p_v}\left(\frac{T}{273K}\right)^{1.81}\right) \tag{3.20}$$

Sorption rate, $\dot{c}$, according concentration based approach, can be calculated as

$$\dot{c} = H_c(c_{bl} - c_b) \tag{3.21}$$

where

$$H_c = \begin{cases} C_1 \exp\left(-C_2\left(\frac{c_b}{c_{bl}}\right)^{C_3}\right) + C_4 & c_b < c_{bl} \\ C_1 \exp\left(-C_2\left(2 - \frac{c_b}{c_{bl}}\right)^{C_3}\right) + C_4 & c_b > c_{bl} \end{cases} \tag{3.22}$$

$$C_2 = c_{21}\exp(c_{22}h) + c_{23}\exp(c_{24}h) \tag{3.23}$$

$$c_{bl} = \rho_0 m_{bl} \tag{3.24}$$

Coefficients C_1, C_2, C_3, C_4 are, in general, realtive humidity dependent. However C_1, C_3, C_4, c_{21}, c_{22}, c_{23}, c_{24} can be used as constants during RH steps. C_3, c_{21}, c_{22}, c_{21}, c_{22}, are non-dimensional whereas C_1, C_4 have the dimension of the inverse of time.
m_bl can be calculated using sorption isotherm, which represent equilibrium

$$m_{bl} = \frac{h}{f_1 + f_2 h + f_3 h^2} \tag{3.25}$$

f_1, f_2, f_3 are parameters depending on wood type and temeperature and are all non-dimensional.

A pressure-based approach for calculating sorption rate also exists but it's not used in the implementation we are reporting.

Transfer coefficient of the boundary layer, k_p, can be calculated as

$$k_p = \frac{M_{H2O} k_v}{RT} \tag{3.26}$$

where

$$k_v = \frac{Sh D_a}{L} \tag{3.27}$$

$$Sh = \begin{cases} 0.66 Re^{0.5} Sc^{0.33} & if\ Re < 16000 \\ 0.036 Re^{0.8} Sc^{0.33} & if\ Re \geq 16000 \end{cases} \tag{3.28}$$

$$Re = \frac{L v_{air} \rho_a}{\mu} \tag{3.29}$$

$$Sc = \frac{\mu}{\rho_a D_a} \tag{3.30}$$

$$\rho_a = \frac{M_{da}(p_{atm} - p_v^a) + M_{H2O} p_v^a}{RT} \tag{3.31}$$

$$\mu = 1.718e-5 + .0049e-5(T - 273.15) \tag{3.32}$$

$$D_a = 2.2e-5 \frac{p_{atm}}{p_v^a + p_{atm}} \left(\frac{T}{273.15} \right)^{1.75} \tag{3.33}$$

Saturated vapor pressure can be calculated with

$$p_s = exp(53.421 - \frac{6516.3}{T} - 4.125 \times ln(T)) \tag{3.34}$$

See the performed simulations description in section **??** to see which values for φ, ρ_0, p_s, T, p_{atm}, C_1, c_{21}, c_{22}, c_{23}, c_{24},C_3, C_4, f_1,f_2, f_3, v_{air}, L, $D_b^L, D_b^T, D_v^0, \xi_L, \xi_T$ have been used.

The algorithm can be enriched with an hysteresis model but that's not the subject of this section.

External flux

The flux of moisture or humidity across the external surface can be described in terms of difference in bound water concentration or in terms of difference in water vapor pressure. In both cases the flux is proportional to the difference of potential between the external ambient and the external surface of the domain, by a coefficient that could be called emission.

Here is the relationship between the coefficient in terms of bound water concentration and the one in terms of water vapor pressure.

$$\Phi = \beta_{p_v} \Delta p_v = \beta_{c_b} \Delta c_b$$

$$\beta_{c_b} = \beta_{p_v} \frac{\Delta p_v}{\Delta c_b} = \beta_{p_v} \frac{p_s}{rho_0 EMC(RH = 1.00)}$$

$$\beta_{p_v} = \beta_{c_b} \frac{\Delta c_b}{\Delta p_v} = \beta_{c_b} \frac{rho_0 EMC(RH = 1.00)}{p_s}$$

Permeance = 1 / Resistance

$$k_p = 2.9e - 124.3e - 8$$

vedi tesi di Davide e Irene pag 66/149 e appendix 4/81

Porosity

Wood is a porous material: its volume consists of a solid volume and a voids volume.

Diffusion of water inside the wood consists of diffusion of bound water and diffusion of water vapor. These two phenomena are coupled by phase change between bound water and water vapor.

Water vapor diffuses through pores.

Vapor diffusion phenomenon is described in terms of concentration or pressure. The relationship between water vapor concentration and water vapor pressure can be obtained by ideal gas equation

$$pV = nRT$$

where V is the volume of voids $V_v = \phi V_{tot}$

Concentration is water vapor mass per unit of total volume $c_v = m_v / V_{tot}$

The relationship between c_v and p_v is so

$$p_v = c_v \frac{RT}{\phi M}$$

where M is water vapor molar mass.

Water vapor diffusion equation without sorption is

$$c_{v,t} = \nabla \bullet (\mathbf{D_v} \nabla c_v)$$

which, being $\frac{RT}{\phi M} = cost$ becomes

$$p_{v,t} = \nabla \bullet (\mathbf{D_v} \nabla p_v)$$

We can use

$$\mathbf{D_v} = \xi 2.31e-5 m^2/s \left(\frac{p_{atm}}{p_{atm}+p_v} \left(\frac{T}{273K} \right)^{1.81} \right) \tag{3.35}$$

where ξ accounts for the wood resistance due to its porous structure and

$$2.31e-5 m^2/s \frac{p_{atm}}{p_{atm}+p_v} \left(\frac{T}{273K} \right)^{1.81}$$

is an empirical expression by Schirmer.
Water vapor diffusion equation with sorption is

$$c_{v,t} = \nabla \bullet (\mathbf{D_v} \nabla c_v) - \dot{c}$$

which, being $\frac{RT}{\phi M} = cost$ becomes

$$p_{v,t} = \nabla \bullet (\mathbf{D_v} \nabla p_v) - \dot{c} \frac{\phi M}{RT}$$

The equation can also be written in terms of the relative humidity $h = p_v/p_s = RH/100$
which being $p_s = cost$

$$h_{,t} = \nabla \bullet (\mathbf{D_v} \nabla h) - \dot{c} \frac{\phi M}{RT} \frac{1}{p_s}$$

3.2 A 3D orthotropic viscoelastic-mechanosorptive creep model for wood

An orthotropic viscoelastic-mechanosorptive material model is specialized on the basis of previous models.

Wood is usually described as a continuum and homogeneous material with cylindrical orthotropy (**?**). This is due to the particular growth mechanism in circular increments which produces the annual rings in the cross section and mainly longitudinally oriented cells (called tracheids at the microscopic level). The anisotropy in the cross sectional plane is due, at least partly, to the growth in radial cell rows which determines unbroken cell wall lines, called wood rays. Furthermore, because of the mainly longitudinally oriented cells, a larger anisotropy between the cross sectional plane and the longitudinal direction is observed. In this work the macroscopic level is defined as the scale of annual ring formation. However, the earlywood and the latewood rings are not considered as different materials. This results in an orthotropic material in which the radial (R) and the tangential (T) axes are oriented in directions where the earlywood and latewood rings are oriented in serial and in parallel directions in the cross section plane. Considering also the grain direction (L), the material at local level is orthotropic. In the Abaqus numerical model used in this paper (see

Section 4) also the influence of the pith (origin) position has been taken into account by using a cylindrical coordinate system and specifying the material orientation as done in (**?**). The influence of cylindrical coordinate systems on the stress calculation has been discussed for example in (**?**). In Fig. 3.1 the cylindrical coordinates in the plane RT are shown.

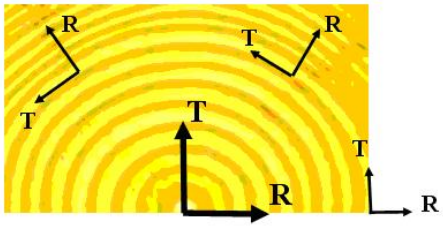

Figure 3.1: Cylindrical coordinates in the plane RT with origin in the pith location.

To analyze timber structures under service conditions of buildings, the changes of moisture content during loading have to be considered. The 3D orthotropic creep model presented in this work takes into account the hygroexpansion effects and the influence of viscoelastic creep and mechanosorption. Both the viscoelastic and the mechanosorptive creep coefficients presented in the next subsections are obtained by fitting the experimental results in the cross grain and in the grain directions provided in **?** and **??**. These creep parameters are considered to be general for the types of wood analyzed in this study.

3.2.1 Thermodynamic formulation of the model

According to **?** and **?**, thermodynamics is a powerful theoretical tool for the formulation of general problems characterized by the interdependence of heat, moisture and deformation. In the present work temperature is assumed to be constant and moisture transfer is considered to be independent of mechanical variables. In this context, the main coupling effects are moisture and moisture change–rate dependence of hygroexpansion strain, and viscoelastic and mechanosorptive strain rates, respectively.

From a rheological point of view, the material model presented in this paper is composed of five deformation mechanisms which provide an additive decomposition of strain into elastic response, hygroexpansion, viscoelastic creep, recoverable mechanosorption and mechanosorptive irrecoverable creep (see Fig. 3.2). Both the viscoelastic and the mechanosorptive recoverable creep are described through Kelvin type elements (**???**). These elements are very suitable for the whole thermodynamic formulation of the problem. The description of irrecoverable strain due to mechanosorption is done by means of the mechanosorptive dashpot scheme proposed in (**?**). The total strain tensor $\boldsymbol{\varepsilon}$ of the model is given

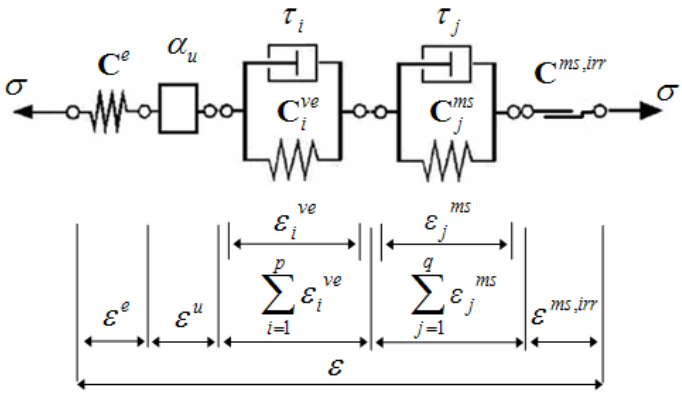

Figure 3.2: Scheme of the rheological constitutive model.

by

$$\boldsymbol{\varepsilon} = \boldsymbol{\varepsilon}^e + \boldsymbol{\varepsilon}^u + \sum_{i=1}^{p} \boldsymbol{\varepsilon}_i^{ve} + \sum_{j=1}^{q} \boldsymbol{\varepsilon}_j^{ms} + \boldsymbol{\varepsilon}^{ms,irr} \tag{3.36}$$

where $\boldsymbol{\varepsilon}^e$ is the elastic strain, $\boldsymbol{\varepsilon}^u$ the hygroexpansion strain, $\boldsymbol{\varepsilon}_i^{ve}$ the elemental viscoelastic strain, $\boldsymbol{\varepsilon}_j^{ms}$ the elemental mechanosorptive strain and $\boldsymbol{\varepsilon}^{ms,irr}$ the irrecoverable part of the total mechanosorptive strain. The terms p and q are the number of viscoelastic Kelvin elements and of the mechanosorptive Kelvin elements, respectively.

In this work the thermodynamic formulation of the constitutive model is based on the general approach proposed by **?**. The starting point is the Helmholtz free energy expressed as a function of temperature T, moisture content u, the total strain tensor $\boldsymbol{\varepsilon}$, the elemental strain tensors $\boldsymbol{\varepsilon}_i^{ve}$ and $\boldsymbol{\varepsilon}_j^{ms}$ and the irrecoverable mechanosorptive strain tensor $\boldsymbol{\varepsilon}^{ms,irr}$:

$$\begin{aligned} \Psi(T, u, \boldsymbol{\varepsilon}, \boldsymbol{\varepsilon}_i^{ve}, \boldsymbol{\varepsilon}_j^{ms}, \boldsymbol{\varepsilon}^{ms,irr}) = \Phi(u,T) + \Phi^e(\boldsymbol{\varepsilon}^e) + \\ \Phi^{ve}(\boldsymbol{\varepsilon}_i^{ve}) + \Phi^{ms}(\boldsymbol{\varepsilon}_j^{ms}) + \Phi^{ms,irr}(\boldsymbol{\varepsilon}^{ms,irr}) \end{aligned} \tag{3.37}$$

$$\text{with } \boldsymbol{\varepsilon}^e = \boldsymbol{\varepsilon} - \boldsymbol{\varepsilon}^u - \textstyle\sum_{i=1}^{p} \boldsymbol{\varepsilon}_i^{ve} - \sum_{j=1}^{q} \boldsymbol{\varepsilon}_j^{ms} - \boldsymbol{\varepsilon}^{ms,irr}$$

where $\Phi(u,T)$ is a general expression for the thermal energy and Φ^e represents the elastic strain energy given by

$$\Phi^e(\boldsymbol{\varepsilon}^e) = \frac{1}{2} \boldsymbol{\varepsilon}^e : \mathbf{C}^e : \boldsymbol{\varepsilon}^e \tag{3.38}$$

being $\mathbf{C}^e$ the elastic stiffness tensor. The terms $\Phi^{ve}(\boldsymbol{\varepsilon}_i^{ve})$ and $\Phi^{ms}(\boldsymbol{\varepsilon}_j^{ms})$ are the energy stored in the viscoelastic elements and the one stored in the mechanosorp-

tive elements, respectively:

$$\Phi^{ve}(\boldsymbol{\varepsilon}_i^{ve}) = \frac{1}{2}\sum_{i=1}^{p} \boldsymbol{\varepsilon}_i^{ve} : \mathbf{C}_i^{ve} : \boldsymbol{\varepsilon}_i^{ve}; \qquad \Phi^{ms}(\boldsymbol{\varepsilon}_j^{ms}) = \frac{1}{2}\sum_{j=1}^{q} \boldsymbol{\varepsilon}_j^{ms} : \mathbf{C}_j^{ms} : \boldsymbol{\varepsilon}_j^{ms} \quad (3.39)$$

where $\mathbf{C}_i^{ve}$ represents the elemental viscoelastic stiffness tensor and $\mathbf{C}_j^{ms}$ the elemental mechanosorptive stiffness tensor. Finally, $\Phi^{ms,irr}(\boldsymbol{\varepsilon}^{ms,irr})$ is the irrecoverable energy related to mechanosorption.

Since this paper presents a finite element analysis, the components of any fourth-order or second–order tensor with respect to a base $\{e_R, e_T, e_L\}$ aligned with axes R-T-L are conveniently rearranged in matrix or vector form following Voigt's notation (**???**). In the next sections the same notations for tensors and matrices are used.

3.2.2 Elastic deformation

The main constitutive equation of the model is obtained by differentiating the free energy of Eq. (3.37) with respect to the total strain tensor and this provides the total stress tensor

$$\boldsymbol{\sigma} := \frac{\partial \Psi}{\partial \varepsilon} = \mathbf{C}^e : \boldsymbol{\varepsilon}^e \quad (3.40)$$

In the case of orthotropic materials as wood, the elastic compliance tensor $\mathbf{C}^{e-1}$ in matrix form is

$$\mathbf{C}^{e-1} = \begin{bmatrix} \frac{1}{E_R} & \frac{-\nu_{TR}}{E_T} & \frac{-\nu_{LR}}{E_L} & 0 & 0 & 0 \\ \frac{-\nu_{RT}}{E_R} & \frac{1}{E_T} & \frac{-\nu_{LT}}{E_L} & 0 & 0 & 0 \\ \frac{-\nu_{RL}}{E_R} & \frac{-\nu_{TL}}{E_T} & \frac{1}{E_L} & 0 & 0 & 0 \\ 0 & 0 & 0 & \frac{1}{G_{RT}} & 0 & 0 \\ 0 & 0 & 0 & 0 & \frac{1}{G_{RL}} & 0 \\ 0 & 0 & 0 & 0 & 0 & \frac{1}{G_{TL}} \end{bmatrix} \quad (3.41)$$

where the Poisson ratios are related as follows:

$$\nu_{RL} = \frac{E_R}{E_L}\nu_{LR}, \quad \nu_{TL} = \frac{E_T}{E_L}\nu_{LT}, \quad \nu_{TR} = \frac{E_T}{E_R}\nu_{RT} \quad (3.42)$$

According to (**?**), both the elastic and the shear moduli are expressed as functions of density, temperature and moisture content:

$$\begin{array}{l} E_i = E_{i,ref}(1 + a_1(\rho - \rho_{ref}) + b_1(T - T_{ref}) + c_1(u - u_{ref})) \\ \text{with} \;\; i = R, T, L \\ G_{ij} = G_{ij,ref}(1 + a_1(\rho - \rho_{ref}) + b_1(T - T_{ref})) + c_1(u - u_{ref})) \\ \text{with} \;\; i, j = R, T, L; \quad i \neq j \end{array} \quad (3.43)$$

$E_{i,ref}$ and $G_{ij,ref}$ being the values of moduli in reference conditions of density ρ_{ref}, temperature T_{ref} and moisture content u_{ref}. In the examples analyzed in this paper, the density is considered to be constant ($\rho = \rho_{ref} = 550$ kg/m^3 for

pine wood and $\rho = \rho_{ref} = 450$ kg/m^3 for spruce wood). Also the temperature is assumed to be constant ($T = T_{ref} = 20^\circ C$). Following (**?**), the moisture content $0 < u < 1$ is expressed as $u = (m - m_0)/m_0$ being m the mass of the specimen and m_0 the mass of the specimen in absolute dry condition. The reference value of moisture content is $u_{ref} = 0.12$. The values of the dimensionless parameters in Eq. (3.43) are $a_1 = 0.0003, b_1 = -0.007, c_1 = 2.6$ (**?**).

Referring to (3.40), the time derivative of the elastic strain is

$$\dot{\boldsymbol{\varepsilon}}^e = \dot{\mathbf{C}}^{e^{-1}} : \boldsymbol{\sigma} + \mathbf{C}^{e-1} : \dot{\boldsymbol{\sigma}} \tag{3.44}$$

where $\dot{\mathbf{C}}^{e^{-1}}$ represents the elastic compliance tensor rate.

3.2.3 Hygroexpansion

The hygroexpansion strain has the following mathematical rate form:

$$\dot{\boldsymbol{\varepsilon}}^u = \boldsymbol{\alpha}_u \dot{u} \tag{3.45}$$

where $\dot{u}$ represents the moisture content rate and $\boldsymbol{\alpha}_u$ is the second–order hygroexpansion tensor which, rewritten in vector form, is $\boldsymbol{\alpha}_u = [\alpha_R, \alpha_T, \alpha_L, 0, 0, 0]^{\mathrm{T}}$. The values of the hygroexpansion coefficients used in this work are those reported in (**?**):

$$\alpha_R = 0.13;\ \alpha_T = 0.27;\ \alpha_L = 0.005 \tag{3.46}$$

It seems that the use of (3.45) in the context of 1D and 2D modelling of wood, is sufficient for fitting the experimental results (**??**). In the present work, this model is used for describing hygroexpansion in the cross grain direction. For the case of timber beams subjected to bending, however, the following expression for the hygroexpansion strain rate component in longitudinal direction is used:

$$\dot{\boldsymbol{\varepsilon}}^u_L = \alpha_L \left(1 - \frac{\beta}{\alpha_L} \varepsilon^{mech}_L\right) \dot{u} \tag{3.47}$$

where ε^{mech}_L is the corresponding component of the mechanical strain vector (which describes total strain excluding hygroexpansion). This equation, proposed in (**?**), was found to describe better the response in the grain direction of wood under compressive, tensile and bending loads. Tensile loads resulted in smaller hygroexpansion strains compared to compression loads. This formulation was only tested at low to moderate load levels, as the interest was on working stress levels of structures. A similar approach was used in (**?**) where the dependence on stress of Eq. (3.45) is also discussed.

3.2.4 Viscoelastic creep

The additional deformation shown by wood under sustained loads in constant moisture conditions is known as viscoelastic creep. The derivative of the Helmholtz

Table 3.1: Dimensionless compliance parameters used for the viscoelastic model.

i	$\boldsymbol{\tau}_i$ [h]	J_i^{ve} [-]
1	2.4	0.085
2	24	0.035
3	240	0.07
4	2400	0.2

free energy in Eq. (3.37) with respect to the elemental viscoelastic strain provides the thermodynamic stress in the i-th Kelvin element (**?**). Using (3.40) the following equation holds:

$$\boldsymbol{\sigma}_i^{ve} := -\frac{\partial \Psi}{\partial \boldsymbol{\varepsilon}_i^{ve}} = \boldsymbol{\sigma} - \mathbf{C}_i^{ve} : \boldsymbol{\varepsilon}_i^{ve} \tag{3.48}$$

and the rate equation for a single viscoelastic element can be written as

$$\dot{\boldsymbol{\varepsilon}}_i{}^{ve} + \frac{1}{\tau_i}\boldsymbol{\varepsilon}_i{}^{ve} = \frac{1}{\tau_i}\mathbf{C}_i^{ve-1} : \boldsymbol{\sigma} \tag{3.49}$$

where τ_i represents the retardation (or characteristic) time of the Kelvin element (**??**). In the present work, the elemental compliance viscoelastic tensor is assumed to be proportional to the elastic compliance in the reference conditions:

$$\mathbf{C}_i^{ve-1} = J_i^{ve}\mathbf{C}^{e-1}(u_{ref}) \tag{3.50}$$

where J_i^{ve} represents a dimensionless viscoelastic compliance ratio compared to the elastic compliance for the i-th element and $u_{ref} = 0.12$. In this paper the dimensionless compliance ratios are calculated on the basis of the viscoelastic model proposed by **?** for wood in the grain direction during constant moisture conditions. The use of the same viscoelastic compliance ratios in R and T directions is a simplification of the model. Four Kelvin elements are considered (the values of retardation times and compliances are reported in Table 3.1). These parameters are used in all moisture conditions for the cases studied in this paper.

As shown in (**?**), for stress driven problems the solution of (3.49) can be written in the following form:

$$\boldsymbol{\varepsilon}_i^{ve} = \boldsymbol{\varepsilon}_{i,n}^{ve} \exp\left(\frac{-\Delta t}{\tau_i}\right) + \int_{t_n}^{t_{n+1}} \frac{\mathbf{C}_i^{ve-1} : \boldsymbol{\sigma}(t)}{\tau_i} \exp\left(-\frac{t_{n+1} - t}{\tau_i}\right) dt \tag{3.51}$$

where $\Delta t = t_{n+1} - t_n$ is the time increment and $\boldsymbol{\varepsilon}_{i,n}^{ve}$ represents the elemental viscoelastic strain tensor calculated at the time t_n.

3.2.5 Mechanosorptive creep

The phenomenon of deformation increase in the presence of changing moisture under mechanical loads is known as mechanosorption. For describing recoverable

mechanosorption, an equation similar to that of the simple viscoelastic creep is used:

$$\dot{\boldsymbol{\varepsilon}}_j^{ms} = \frac{\mathbf{C}_j^{ms-1} : \boldsymbol{\sigma} - \boldsymbol{\varepsilon}_j{}^{ms}}{\tau_j} |\dot{u}| \tag{3.52}$$

where τ_j is a material parameter comparable to a retardation time in viscoelasticity (**?**). This parameter is dimensionless and independent of moisture (see **?**). The solution of (3.52) is of the same form as (3.51) but moisture content u is used instead of time:

$$\boldsymbol{\varepsilon}_j^{ms} = \boldsymbol{\varepsilon}_{j,n}^{ms} \exp\left(\frac{-\Delta u^a}{\tau_j}\right) + \int_{t_n}^{t_{n+1}} \frac{\mathbf{C}_j^{ms-1} : \boldsymbol{\sigma}(t)}{\tau_j} \exp\left(-\frac{u_{n+1}^a - u^a(t)}{\tau_j}\right) dt \tag{3.53}$$

where $\Delta u = u_{n+1}^a - u_n^a$ with $u^a = |u|$ and $\boldsymbol{\varepsilon}_{j,n}^{ms}$ represents the elemental mechanosorptive strain tensor calculated at the time t_n. The elemental mechanosorptive compliance tensor in matrix form is assumed to be the following:

$$\mathbf{C}_j^{ms-1} =$$

$$\begin{bmatrix}
\frac{m_j^{ms,T} E_T}{E_R} & -m_j^{ms,T}\nu_{TR} & -\frac{m_j^{ms,T}\nu_{LR} E_T}{E_L} & 0 & 0 & 0 \\
-\frac{m_j^{ms,T}\nu_{RT} E_T}{E_R} & m_j^{ms,T} & -\frac{m_j^{ms,T}\nu_{LT} E_T}{E_L} & 0 & 0 & 0 \\
-\frac{m_j^{ms,T}\nu_{RL} E_T}{E_R} & -m_j^{ms,T}\nu_{TL} & m_j^{ms,L} & 0 & 0 & 0 \\
0 & 0 & 0 & \frac{m_j^{ms,T} E_T}{G_{RT}} & 0 & 0 \\
0 & 0 & 0 & 0 & \frac{m_j^{ms,T} E_T}{G_{RL}} & 0 \\
0 & 0 & 0 & 0 & 0 & \frac{m_j^{ms,T} E_T}{G_{TL}}
\end{bmatrix} \tag{3.54}$$

The coefficients of this matrix are based on: *a*) the model for mechanosorption in cross grain section proposed by **?** and *b*) the mechanosorptive model for wood parallel to grain introduced by **?**. Starting from the mechanosorptive compliance in tangential direction $m_j^{ms,T}$ the other coefficients of $\mathbf{C}_j^{ms-1}$ are obtained by using the ratios between the respective terms of the elastic matrix. However, term $m_j^{ms,L}$ represents a fraction of a reference elastic compliance in longitudinal direction defined as

$$m_0^{ms,L} = \frac{0.7}{E_L(u_{0,ref})} \ [1/\text{MPa}] \tag{3.55}$$

where $u_{0,ref} = 0.20$.

As in the 1D model of **?**, the mechanism for recoverable mechanosorption is composed of three Kelvin elements. Since the full constitutive model presented in the present work is three-dimensional and the influence of the viscoelastic creep is taken into account, the values of the tangential compliance are found to be different from those of the previous 1D model. The same mechanosorptive compliances are used for analyzing all tests described in this work. The values of these compliances and the corresponding retardation times are listed in Table 3.2.

Table 3.2: Tangential and longitudinal compliance parameters for the recoverable mechanosorptive part of the model.

i	$\boldsymbol{\tau}_i$ [-]	$m_j^{ms,T}$ [1/MPa]	$m_j^{ms,L}$ [1/MPa]
1	0.01	0.0006	0.25 $m_0^{ms,L}$
2	0.1	0.0006	0.7 $m_0^{ms,L}$
3	1.0	0.005	0.05 $m_0^{ms,L}$

Following **?**, a further mechanism for describing irrecoverable mechanosorption is added and the expression for the irrecoverable rate is assumed to be

$$\dot{\boldsymbol{\varepsilon}}^{ms,irr} = \mathbf{C}^{ms,irr\,-1} : \boldsymbol{\sigma} \mid \dot{U} \mid \tag{3.56}$$

where the moisture content rate $\dot{U}$ refers to the moisture levels not reached during the previous strain history. The irrecoverable mechanosorptive matrix is assumed to be the following:

$$\mathbf{C}^{ms,irr\,-1} = \begin{bmatrix} m_v \frac{E_T}{E_R} & -m_v \frac{E_T}{E_R}\nu_{RT} & 0 & 0 & 0 & 0 \\ -m_v \frac{E_T}{E_R}\nu_{RT} & m_v & 0 & 0 & 0 & 0 \\ 0 & 0 & 0 & 0 & 0 & 0 \\ 0 & 0 & 0 & m_v \frac{E_T}{G_{RT}} & 0 & 0 \\ 0 & 0 & 0 & 0 & m_v \frac{E_T}{G_{RL}} & 0 \\ 0 & 0 & 0 & 0 & 0 & m_v \frac{E_T}{G_{TL}} \end{bmatrix} \tag{3.57}$$

where the value of the irrecoverable coefficient m_v in tangential direction, obtained by fitting the experimental results, is $m_v = 0.066\,\mathrm{MPa}^{-1}$. The other coefficients of $\mathbf{C}^{ms,irr\,-1}$ are calculated from m_v by using the elastic matrix ratios. Equation (3.56) shows that the deformation due to irrecoverable mechanosorption is considered to be stress rate independent, that is, at a rheological level a mechanosorptive dashpot scheme is used **?**. In some earlier studies mechanosorptive dashpot schemes for describing the full mechanosorptive phenomenon were used (**??**). In the presence of elevated temperatures which may introduce relevant irrecoverable deformations, this approach may not be anymore sufficient and additional Kelvin plastic elements are needed in the rheological scheme (**?**).

3.2.6 Elastic strain increment

The elastic strain increment is composed of two parts coming from the finite increment form of the elastic rate equation (3.44):

$$\Delta\boldsymbol{\varepsilon}^{e}_{n+1} = \Delta\boldsymbol{\varepsilon}^{e,\sigma_n}_{n+1} + \Delta\boldsymbol{\varepsilon}^{e,\Delta t}_{n+1} \tag{3.58}$$

with

$$\Delta\boldsymbol{\varepsilon}^{e,\sigma_n}_{n+1} = \dot{\mathbf{C}}^{e^{-1}} : \boldsymbol{\sigma}_n \Delta t \tag{3.59}$$

$$\Delta\boldsymbol{\varepsilon}^{e,\Delta t}_{n+1} = \mathbf{C}^{e-1} : \dot{\boldsymbol{\sigma}}_{n+1} \Delta t \tag{3.60}$$

In the used model, the moisture content rate is assumed to have a constant value during each time increment Δt. By using relationships (3.43) for the elastic moduli in the case of constant density and temperature, the following equation holds (see also **?**):

$$\Delta\boldsymbol{\varepsilon}_{n+1}^{e,\sigma_n} = -\frac{b_1 \Delta u_{n+1}}{1 + b_1(u_{n+1} - u_{ref})} \mathbf{C}^{e-1} : \boldsymbol{\sigma}_n \tag{3.61}$$

where the moisture content increment is defined as $\Delta u_{n+1} = u_{n+1} - u_n$.

A linear relationship is assumed during each time increment so that the increment of the elastic strain depending on Δt at the current time step is

$$\Delta\boldsymbol{\varepsilon}_{n+1}^{e,\Delta t} = \mathbf{C}^{e-1} : \Delta\boldsymbol{\sigma}_{n+1} \tag{3.62}$$

where $\Delta\boldsymbol{\sigma}_{n+1}$ has to be calculated by the algorithm of moisture induced stress update.

3.2.7 Hygroexpansion strain increment

Starting from (3.45), the increment of hygroexpansion strain is directly dependent on the moisture increment:

$$\Delta\boldsymbol{\varepsilon}_{n+1}^{u} = \boldsymbol{\alpha}\Delta u_{n+1} \tag{3.63}$$

When rate equation (3.47) is used for describing hygroexpansion in the longitudinal direction, the corresponding increment of strain is evaluated as

$$\Delta\varepsilon_{L,n+1}^{u} = \alpha_L \left(1 - \frac{\beta}{\alpha_L}\varepsilon_{L,n}^{mech}\right) \Delta u_{n+1} \tag{3.64}$$

3.2.8 Recoverable creep strain increments

By integrating the equation of viscoelastic creep during the time for the i-th Kelvin element, the following increment of elemental viscoelastic strain is obtained:

$$\Delta\boldsymbol{\varepsilon}_{i,n+1}^{ve} = \mathbf{C}_{i,n+1}^{ve^{-1}} : \Delta\boldsymbol{\sigma}_{n+1} - \mathbf{R}_{i,n}^{ve}(\boldsymbol{\varepsilon}_{i,n}^{ve}, \boldsymbol{\sigma}_n) \tag{3.65}$$

where $\mathbf{C}_{i,n+1}^{ve}$ is the algorithmic viscoelastic tangent operator:

$$\mathbf{C}_{i,n+1}^{ve} = \frac{\mathbf{C}_i^{ve}}{\mathbb{T}_{n+1}(\xi_i)} \tag{3.66}$$

with $\xi_i = \frac{\Delta t}{\tau_i}$, $\mathbb{T}_{n+1}(\xi_i) = 1 - \frac{1}{\xi_i}[1 - \exp(-\xi_i)]$ and $\mathbf{R}_{i,n}^{ve}$ is a function of the strain $\boldsymbol{\varepsilon}_{i,n}^{ve}$ and stress $\boldsymbol{\sigma}_n$ at the previous time step (see **?** for more detail on this computational approach):

$$\mathbf{R}_{i,n}^{ve} = [\boldsymbol{\varepsilon}_{i,n}^{ve} - \mathbf{C}_i^{ve^{-1}} : \boldsymbol{\sigma}_n][1 - \exp(-\xi_i)] \tag{3.67}$$

Since the equation for mechanosorption is analogous to that of viscoelastic creep, a similar finite increment for the j-th Kelvin element is obtained:

$$\Delta\boldsymbol{\varepsilon}^{ms}_{j,n+1} = \mathbf{C}^{ms^{-1}}_{j,n+1} : \Delta\boldsymbol{\sigma}_{n+1} - \mathbf{R}^{ms}_{j,n}(\boldsymbol{\varepsilon}^{ms}_{j,n}, \boldsymbol{\sigma}_n) \tag{3.68}$$

where $\mathbf{C}^{ms}_{j,n+1}$ is the algorithmic mechanosorptive tangent operator:

$$\mathbf{C}^{ms}_{j,n+1} = \frac{\mathbf{C}^{ms}_{j}}{\mathbb{T}_{n+1}(\xi_j)} \tag{3.69}$$

being $\xi_j = \frac{\Delta u}{\tau_j}$, $\mathbb{T}_{n+1}(\xi_j) = 1 - \frac{1}{\xi_j}[1 - \exp(-\xi_j)]$ and $\mathbf{R}^{ms}_{j,n}$ a function of $\boldsymbol{\varepsilon}^{ms}_{j,n}$ and $\boldsymbol{\sigma}_n$ at the previous time step:

$$\mathbf{R}^{ms}_{j,n} = [\boldsymbol{\varepsilon}^{ms}_{j,n} - \mathbf{C}^{ms^{-1}}_{j} : \boldsymbol{\sigma}_n][1 - \exp(-\xi_j)] \tag{3.70}$$

3.2.9 Irrecoverable mechanosorptive creep strain increment

The increment due to irrecoverable mechanosorption depends on both the moisture increment and the stress at the beginning of the time step:

$$\Delta\boldsymbol{\varepsilon}^{ms,irr}_{n+1} = \mathbf{C}^{ms,irr^{-1}} : \boldsymbol{\sigma}_n|\Delta U| \tag{3.71}$$

In the above equation, $\Delta U = U_{n+1} - U_n$ with $U_{n+1} = u_{n+1}$ and $U_n = u_{1,n}$ where $u_{1,n}$ represents the value of moisture content u_n not yet reached during the previous strain history. Finally, $\Delta U = 0$ for all U_n already reached.

3.2.10 Tangent operator of the model

Starting from the incremental form of the total strain (5.4) and taking into account (3.61), (3.62), (3.65) and (3.68), the following equation holds:

$$\mathbf{C}^{-1}_{\mathrm{T}} : \Delta\boldsymbol{\sigma}_{n+1} = \Delta\boldsymbol{\varepsilon}_{n+1} - \Delta\boldsymbol{\varepsilon}^{e,\sigma_n}_{n+1} - \Delta\boldsymbol{\varepsilon}^{u}_{n+1} - \Delta\boldsymbol{\varepsilon}^{ms,irr}_{n+1} + \sum_{i=1}^{p}\mathbf{R}^{ve}_{i,n} + \sum_{j=1}^{q}\mathbf{R}^{ms}_{j,n} \tag{3.72}$$

where $\mathbf{C}_{\mathrm{T}}$ represents the algorithmic tangent operator of the whole model:

$$\mathbf{C}_{\mathrm{T}} = \left(\mathbf{C}^{e^{-1}} + \sum_{i=1}^{p}\mathbf{C}^{ve^{-1}}_{i,n+1} + \sum_{j=1}^{q}\mathbf{C}^{ms^{-1}}_{j,n+1}\right)^{-1} \tag{3.73}$$

Chapter 4

Algorithms

The computational approach presented in the reference is validated by analyzing some wood tests described in the literature and comparing the computational results with the reported experimental data.

4.1 Moisture stress analysis

The description of the algorithm used for modelling moisture diffusion in wood and the details of its implementation in ABAQUS® FE code, are given in the following.

4.1.1 Sequential Analysis

Let's rewrite basis equations in the simplest form:

$$\frac{\partial}{\partial t}(c_b) = \nabla \bullet (\mathbf{D_b}(c_b)\nabla c_b) + \dot{c} \tag{4.1}$$

$$\frac{\partial}{\partial t}(c_v) = \nabla \bullet (\mathbf{D_v}(c_v)\nabla c_v) - \dot{c} \tag{4.2}$$

The scheme of the sequential analysis implemented is

1. Evaluation of $c_v(t)$ and $c_b(t)$, by equation (3.13) and the approximated calculation
$$c_b(t + \Delta t) = c_b(t) + \dot{c}\Delta t$$
2. Evaluation of $c_b(t)$, by equation (3.12) and the value of $c_v(t)$ calculated in the previous step
3. Evaluation of $c_v(t)$ by equation (3.13) and the value of $c_b(t)$ calculated in the previous step
4. repeat 2-3 till convergence to experimental results

These steps are all performed by an ABAQUS® uncoupled heat transfer analysis. Then an ABAQUS® uncoupled stress analysis is performed reading as predefined field moisture calculated in the previous step.

4.1.2 Derivatives

We have to determine the derivative with respect to the unknown of the external surface flux and the one of the internal volume flux.

Derivative of the external surface flux with respect to h

The external surface flux in the diffusion problem is the one described in equation 3.15. But what we have to implement is the external surface flux according to ABAQUS® procedure, i.e. $-\mathbf{n} \bullet (\mathbf{K} \bullet \nabla T) = f$. So according to table 5.1 we need:

$$f_{,h} = k_p \rho_0 \frac{1}{\frac{\varphi M_{H_2O}}{RT}} \tag{4.3}$$

Derivative of the internal volume flux with respect to h

The internal volume flux in the diffusion problem is the one described in equation 3.21. But what we have to implement is the internal volume flux according to ABAQUS® procedure, i.e. q. So according to table 5.1 we need:

$$q_{,h} = \pm \dot{c}_{,h} \rho_0 \frac{1}{p_s} \frac{1}{\frac{\varphi M_{H_2O}}{RT}} \tag{4.4}$$

$$\dot{c}_{,h} = H_{c,h}(c_{bl} - c_b) + H_c c_{bl\,,h} \tag{4.5}$$

$$H_{c,h} = CC(-C_{2\,,h} BB - C_2 BB_{,h}) \tag{4.6}$$

$$CC = C_1 exp(-C_2 BB) \tag{4.7}$$

$$BB = (\frac{c_b}{c_{bl}})^{\pm C_3} \tag{4.8}$$

$$BB_{,h} = \pm C_3 c_b^{\pm C_3} c_{bl}^{\mp C_3 - 1} c_{bl\,,h} \tag{4.9}$$

$$C_{2\,,h} = c_{22} c_{21} exp(c_{22} h) + c_{24} c_{23} exp(c_{24} h) \tag{4.10}$$

$$c_{bl\,,h} = \rho_0 * (AA - h(f_2 + 2 f_3 h))/(AA^2) \tag{4.11}$$

$$AA = (f_1 + f_2 h + f_3 h^2) \tag{4.12}$$

Derivative of the internal volume flux with respect to m

$$q_{,m} = \pm \dot{c}_{,m} \rho_0 \frac{1}{p_s} \frac{1}{\frac{\varphi M_{H_2O}}{RT}} \tag{4.13}$$

$$\dot{c}_{,m} = H_{c,m}(c_{bl} - c_b) - H_c \rho_0 \tag{4.14}$$

$$H_{c,m} = -CCC_2 BB_{,m} \tag{4.15}$$

$$CC = C_1 exp(-C_2 BB) \tag{4.16}$$

$$BB = (\frac{c_b}{c_{bl}})^{\pm C_3} \tag{4.17}$$

$$BB_{,m} = \pm C_3 c_{bl}^{\mp C_3} c_b^{\pm C_3 - 1} \tag{4.18}$$

4.1.3 Formulation

As you can see in **?**

$$\int_V \rho \, \dot{U} = \int_S q + \int_V r \tag{4.19}$$

$$q = -\mathbf{f} \cdot \mathbf{n} \tag{4.20}$$

$$\int_S \mathbf{f} \cdot \mathbf{n} = \int_V div(\mathbf{f}) \tag{4.21}$$

Let´s consider that 4.19+4.20+4.21 give

$$\int_V \rho \, \dot{U} = -\int_V div(\mathbf{f}) + \int_V r \tag{4.22}$$

As you can see at **?**

$$\mathbf{f} = -\mathbf{K} grad(\theta) \tag{4.23}$$

Now, let´s consider that 4.22+4.23 give

$$\rho \, \dot{U} - div(\mathbf{K} grad(\theta)) - r = 0 \tag{4.24}$$

and that 4.20+4.23 give

$$q = \mathbf{K} grad(\theta) \cdot \mathbf{n} \tag{4.25}$$

As you can see in **?**

$$\int_V \delta\theta div(\mathbf{f}) = -\int_V grad(\delta\theta) \cdot \mathbf{f} + \int_S \delta\theta \, \mathbf{f} \cdot \mathbf{n} \tag{4.26}$$

Finally we can obtain that 4.22+4.26 give

$$\int_V \delta\theta \; \rho \; \dot{U} = \int_V grad(\delta\theta) \cdot (\mathbf{f}) + \int_V \delta\theta \; r + \int_S \delta\theta \; q \qquad (4.27)$$

Chapter 5

Abaqus Implementation

The computational tool presented in this document is validated by analyzing some wood tests described in the literature and comparing the computational results with the reported experimental data.

5.1 Moisture stress analysis: ABAQUS® implementation

5.1.1 ABAQUS® analysis procedure

The analysis procedure, that has been used in the implementation, is the Uncoupled Heat Transfer Analysis. The equations of this analysis procedure are:

$$\rho c \frac{\partial \theta}{\partial t} = div(\mathbf{K} \bullet \nabla\theta) + r, \qquad on \quad \Omega \tag{5.1}$$

$$\mathbf{n} \bullet (\mathbf{K} \bullet \nabla\theta) = q, \qquad on \quad \partial\Omega \tag{5.2}$$

$$\theta = \bar{\theta}, \qquad on \quad \partial\Omega \tag{5.3}$$

This procedure has been used for each step of the sequential analysis. Obviously it should be considered $c = 1$, $\rho = 1$ and the matching showed in tabel 5.1.

5.1.2 Sequential Analysis: ABAQUS® implementation

The sequential analysis proposed has been performed, writing to the results file (.fil is the extention for an ABAQUS® Standard job) the unknown solution of a job and then reading this solution in the next job. To this aim the following ABAQUS® input options have been used

ABAQUS® Procedure	θ	r	$\mathbf{K}$	q
Vapor Equation	h	$-\dot{c}\frac{1}{p_s}\frac{1}{\frac{\varphi M_{H_2O}}{RT}}$	$\mathbf{D_v}$	$-k_p(h^s-h^a)\frac{1}{\frac{\varphi M_{H_2O}}{RT}}$
Bound Water Equation	m	$+\dot{c}/rho_0$	$\mathbf{D_b}$	0

Table 5.1: How the ABAQUS® Analysis type has been actually used

***Node File** and ***El File.** To write the solution which will be used in the next analysis.

***FIELD.** To read and use the other phase solution calculated in the previous analysis.

The options used in the input file for writing the solution needed in the next step analysis are

- for the first step analysis, and

  ```
  **
  *** write to results file .fil to read in the next analysis
  ***
  **EL FILE, POSITION=NODES
  SDV
  ```

- for the next to first steps analyses.

  ```
  **
  *** write to results file .fil to read in the next analysis
  ***
  **NODE FILE
  NT
  ```

The template of the option used in the input file for reading the solution needed from the previous step analysis is

```
**
*** read from results file .fil of the previous analysis
***
**FIELD, VARIABLE=1, FILE=<file name>, BSTEP=1, BINC=1,
ESTEP=1, EINC=<number of increments>
```

5.1.3 Material description

The material description has been achieved by using *MATERIAL, which is an ABAQUS® input option. First of all calculation of diffusivity coefficients with third-party software (Ms Excel®) so the results were put in as concuctivity coefficients.

Actually an orthotrope material should be used. But since simulations used are one direction flow, we used a isotrope material, putting only transversal diffusivity.

***Conductivity** It is used for the diffusivity.

***Specific Heat.** It must be set to 1.0 with the data line,

***Density** It should be set to 1,0 or ρ_0 respectively if the unknown is the vapor or the bound-water.

***Depvar.** The number of state variables used is passed in with the data lines of the option. We need only one state variable.

***Heat generation** It is used to call the subroutine used to define the sorption term.

5.1.4 ABAQUS® User Subroutine Interface

The following User subroutines have been implemented:

HETVAL allows you to define a heat flux (sorption rate) due to internal heat generation for heat transfer analysis Concentration-based sorption rate calculation

DFLUX. Neumann boundary condition varying with solution and time

SDVINI. To set m_0 in the first step analysis

DISP. Dirichlet boundary condition varying with time

Even if we have differences in source code between first step, even and odd after 1st ones, we use the same user file as user subroutines source code for both of them. So we don‘t have to write same things more than once without trying to use more than one ABAQUS® user file for a single job.

Hetval subroutine

- Assignment to constants ρ_0, p_s, T, φ, M_{H_2O}.
- Assignment to h,
- Calculation of c_b and p_v,
- Calculation of the coefficent of $\dot{c}$,

- Calculation of c_{bl} and its derivatives with respect to c_b and p_v,
- Calculation of H_c and its derivatives with respect to c_b and p_v,
- Calculation of $\dot{c}$ and its derivative with respect to m or h,
- Calculation of the flux and its derivative with respect to m or h,
- Updating m (if we are in the first sequential step).

Sdvini subroutine

- Assignment of initial value to m (if we are in the first sequential step).

Dflux subroutine

- Assignment to constants ρ_0, p_s, T, φ, M_{H_2O}, R, p_{atm}, ν, L,
- Interpolation of RH,
- Calculation of the flux and its derivative with respect to h.

5.1.5 Units

The units of q are $\frac{kg}{m^3 hours}$ and the units of f are $\frac{kg}{m^2 hours}$.

In the code list of the implementation we have only a conversion factor of 3600 to go from hours to seconds and from $\frac{1}{seconds}$ to $\frac{1}{hours}$ and a conversion factor of $\frac{1}{3600}$ to do the reverse ways.

5.2 A 3D orthotropic viscoelastic-mechanosorptive creep model for wood

Both the constitutive model and the equations needed to describe the moisture flow across the structure are implemented into user subroutines of the Abaqus finite element code and a coupled moisture-stress analysis is performed for several types of mechanical loads and moisture changes.

In the subroutine DFLUX, both the flow magnitude and the rate of change of flow with respect to the current moisture content are calculated.

5.2.1 An algorithm for moisture-induced stress update

From a computational point of view, the problem of creep in wood can be solved by using an incremental analysis during time which takes into account the coupling of moisture changes and stresses. The solution in terms of strain, stress and moisture at a given time $t = t_n$ is assumed to be known while the solution at the current time $t = t_{n+1}$ has to be determined. For each deformation

mechanism the algorithmic tangent operator, based on the correspondent numerical integration scheme, is built as done in (**?**). The single operators are then assembled in a total algorithmic tangent operator.

Let $\Delta\varepsilon_{n+1}$ be the total strain increment at time $t = t_{n+1}$ and $\Delta t = t_{n+1} - t_n$ the time increment. Equation (3.36) can be rewritten in terms of finite increments as

$$\Delta\boldsymbol{\varepsilon}_{n+1} = \Delta\boldsymbol{\varepsilon}^{e}_{n+1} + \Delta\boldsymbol{\varepsilon}^{u}_{n+1} + \sum_{i=1}^{p} \Delta\boldsymbol{\varepsilon}^{ve}_{i,n+1} + \sum_{j=1}^{q} \Delta\boldsymbol{\varepsilon}^{ms}_{j,n+1} + \Delta\boldsymbol{\varepsilon}^{ms,irr}_{n+1} \tag{5.4}$$

The total strain increment $\Delta\boldsymbol{\varepsilon}_{n+1}$ is composed of a part due to hygroexpansion ($\Delta\boldsymbol{\varepsilon}^{u}_{n+1}$) and of two further parts: one dependent on the stress state at the beginning of the time increment ($\Delta\boldsymbol{\varepsilon}^{\sigma_n}$) and the other being a function of the time increment ($\Delta\boldsymbol{\varepsilon}^{\Delta t}$). For the model presented in this work, these two parts of the strain increment are:

$$\Delta\boldsymbol{\varepsilon}^{\sigma_n}_{n+1} = \Delta\boldsymbol{\varepsilon}^{e,\sigma_n}_{n+1} + \boldsymbol{\varepsilon}^{ms,irr}_{n+1} \tag{5.5}$$

$$\Delta\boldsymbol{\varepsilon}^{\Delta t}_{n+1} = \Delta\boldsymbol{\varepsilon}^{e,\Delta t}_{n+1} + \sum_{i=1}^{p} \Delta\boldsymbol{\varepsilon}^{ve}_{i,n+1} + \sum_{j=1}^{q} \Delta\boldsymbol{\varepsilon}^{ms}_{j,n+1} \tag{5.6}$$

The strain increments of Eq. (5.4) as well as the total algorithmic operator of the constitutive model are derived in the Appendix at the end of this paper.

5.2.2 Implementation into the UMAT subroutine of Abaqus

In this work the algorithm for moisture induced stress update is implemented into the user subroutine UMAT of Abaqus code.

At the beginning of the current time step t_{n+1}, the moisture content u_{n+1}, the moisture increment Δu_{n+1} and the total strain increment $\Delta\boldsymbol{\varepsilon}_{n+1}$ have the values calculated by the moisture–stress analysis performed by the program Abaqus/Standard. The value of the strain increment $\Delta\boldsymbol{\varepsilon}_{n+1}$ is given by the variable DSTRAN of the UMAT subroutine. The values of total stress, elemental viscoelastic strain and elemental mechanosorptive strain at the beginning of the current step are equal to those provided by the UMAT subroutine at the end of the previous time step t_n. In particular, the value of the total stress is given by the UMAT variable STRESS while the values of creep strain increments are stored into the UMAT array STATEV.

For sake of generality, at the beginning of the current time step, the stress is indicated as $\boldsymbol{\sigma}^{(k=0)}_{n+1}$, the viscoelastic strain $\boldsymbol{\varepsilon}^{ve^{(k=0)}}_{i,n+1}$ and the mechanosorptive strain $\boldsymbol{\varepsilon}^{ms^{(k=0)}}_{j,n+1}$. Then, the algorithm at the current time step t_{n+1} can be schematically listed in the following way:

1. The elastic compliance matrix $\mathbf{C}^{e\,-1}$, the irrecoverable mechanosorptive matrix $\mathbf{C}^{ms,irr\,-1}$ and the strain increments $\Delta\boldsymbol{\varepsilon}^{\sigma_n}_{n+1}$ and $\Delta\boldsymbol{\varepsilon}^{u}_{n+1}$ are computed.

2. The elemental algorithmic tangent operators for viscoelastic creep and mechanosorption $\mathbf{C}^{ve}_{i,n+1}, \mathbf{C}^{ms}_{j,n+1}$ (based on the elemental matrices $\mathbf{C}^{ve\,-1}_{i}, \mathbf{C}^{ms\,-1}_{j}$) and the tangent operator of the model $\mathbf{C}^{\mathrm{T}}$ are calculated (see Appendix). This last operator will be used by Abaqus/Standard during the moisture–stress analysis.

3. The new stress increment $\Delta\boldsymbol{\sigma}_{n+1}$ and the creep strain increments $\Delta\boldsymbol{\varepsilon}^{ve}_{n+1}$ and $\Delta\boldsymbol{\varepsilon}^{ms}_{n+1}$ are calculated (see Appendix).

4. The updated values of total stress, viscoelastic strain and recoverable mechanosorptive strain are evaluated as

$$\boldsymbol{\sigma}^{(k+1)}_{n+1} = \boldsymbol{\sigma}^{(k)}_{n+1} + \Delta\boldsymbol{\sigma}_{n+1} \tag{5.7}$$

$$\boldsymbol{\varepsilon}^{ve^{(k+1)}}_{i,n+1} = \boldsymbol{\varepsilon}^{ve^{(k)}}_{i,n+1} + \Delta\boldsymbol{\varepsilon}^{ve}_{i,n+1} \tag{5.8}$$

$$\boldsymbol{\varepsilon}^{ms^{(k+1)}}_{j,n+1} = \boldsymbol{\varepsilon}^{ms^{(k)}}_{j,n+1} + \Delta\boldsymbol{\varepsilon}^{ms}_{j,n+1} \tag{5.9}$$

   - In the presence of strong nonlinearities and for more complex constitutive models, the scheme can be repeated from step 3) until $\parallel \mathbf{R}^{(k+1)}_{n+1} \parallel < TOL$, where $\mathbf{R}^{(k+1)}_{n+1}$ is a vector having as components the residual vectors coming from new forms of equations (3.58), (3.65) and (3.68) shown in the Appendix and TOL is a suitable tolerance. This approach was used in (**?**) where a plastic Kelvin element was also introduced for cases of drying under elevated temperatures.

5. The final values of $\boldsymbol{\varepsilon}^{ve^{(k+1)}}_{i,n+1}$ and $\boldsymbol{\varepsilon}^{ms^{(k+1)}}_{j,n+1}$ are stored in the array STATEV of the UMAT subroutine and used for calculating the new quantities of the next time step.

Extension of the method for evaluation of hygrothermal stresses by Abaqus

The algorithm described above can be directly used in the context of a more general analysis for evaluating the stresses induced by both temperature and moisture changes in cases where the influence of temperature is important as, for example, the case of high–temperature drying modelling. This kind of analysis can be performed with Abaqus by using a sequentially coupled method aimed to model both heat and moisture transfer and the induced stresses. The sequential analysis is basically performed in two steps:

1. a transient heat transfer analysis is conducted in order to simulate the temperature field, which is independent of the moisture field;

2. the coupled moisture–stress analysis described in the present work is performed but this time the mechanical quantities are dependent also on the temperature field calculated at step 1.

Table 5.2: Material properties for Scots Pine (*Pinus sylvestris*) used in the analysis.

E_R (MPa)	E_T (MPa)	E_L (MPa)	ν_{RT}	ν_{RL}	ν_{TL}	G_{RT} (MPa)	G_{RL} (MPa)	G_{TL} (MPa)
900	500	12000	0.558	0.038	0.015	40	700	700

In the Abaqus code, the results of the first analysis can be easily read by writing suitable instructions into the input data file of the second analysis. This approach will be presented in detail in a further joint paper by the present authors.

5.2.3 Validation of the model

An important part of this present paper is the validation of the presented 3D model for wood by comparisons with experimental results. The experimental data refer to small size timber specimens. The aim of this numerical work is to verify if the model is suitable for simulating both short-term and long-term deformations and stresses in the presence of moisture variations.

The geometrical models are created by means of the CAE module of Abaqus, Version 6.5-3 (**?**). A local cylindrical coordinate system for wood is given and a cylindrical material orientation is assigned (**?**). The examples studied in the present paper concern straight wood members. Instead, in the case of curved beams, since the piths of the wood parts run along a series of circular arcs, a further Abaqus user subroutine, ORIENT, has to be used in order to define the local material directions (**???**).

The simulations performed in this work are carried out by using the Abaqus/Standard program. To mesh the wood parts, 3D coupled elements available for the temperature–displacement type analyses, i.e. the linear C3D8T or the quadratic C3D20T, are used.

5.2.4 Comparisons with the Toratti and Svensson results (2000, 2002)

Comparisons with the Toratti and Svensson results (2000, 2002) in the direction perpendicular to grain.

The reference experimental data used in this work were obtained by **??** by using clear heartwood samples (10×20 mm^2 cross–section) of Scots pine (*Pinus sylvestris*). Before testing, the specimens were conditioned at room temperature ($T = 20^\circ$ C) and relative humidity RH=60% for 1 year. Several tests under different humidity cycles were performed. In each test, six of the specimens were used for constant compressive load tests, five for constant tensile load tests and one as a free shrinkage reference. Both the loading and the measuring direction coincide with the tangential direction of the wood for all the studied

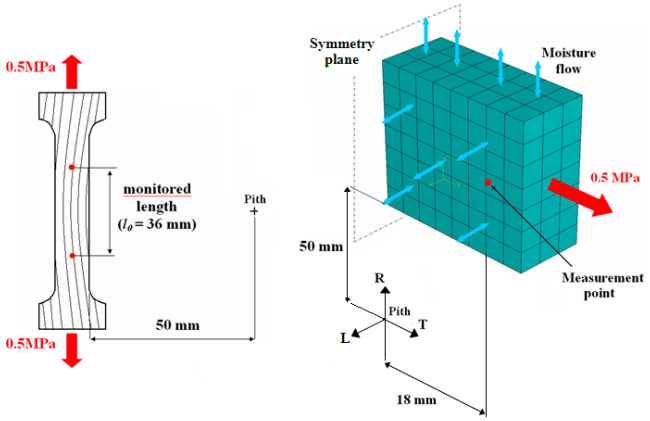

Figure 5.1: Test **??**. Left: geometry of the specimen. Right: Abaqus model and material coordinate system.

specimens. The free shrinkage strain was subtracted from both the tensile and the compressive strain results (shrinkage–corrected strain). The values of the material properties used for the analysis are reported in Table 5.2.

For the numerical simulation, 168 quadratic elements C3D20T are used. In Fig. 5.1 the scheme of the Toratti and Svensson specimen for the constant tensile load tests and the specimen model analyzed by Abaqus are shown.

Short–term analysis

These tests were carried out at different climate cycles (RH versus time) in both high humidity (RH=60–90%) and low humidity (RH=60–45%) conditions. Fast humidity cycle (step-cycle) and slow humidity cycles (triangular cycle) were tested. The specimens were loaded by a moderate tensile or compressive stress of 0.5 MPa and unloaded after 168 hours. Single humidity cycles were applied. During the loading time, a first humidity cycle was imposed for checking its effect on the strain distribution. After unloading, the second humidity cycle was imposed for an other week in order to study the induced recovery. The experimental results for the tension case showed that the deformations during wetting are mostly influenced by the mechanosorptive effect with respect to those during drying, where this effect is not evident. On the contrary, in the compression case, the influence of mechanosorption can be noticed also during drying. Furthermore, the induced deformations were found to be only partially recovered after unloading. Fig. 5.2 shows the comparisons between computational and experimental shrinkage-corrected strains and relative creep curves in case of high humidity cycles for short–term analysis and tensile load test with step-cycle humidity. The reported experimental data is the mean value of six tensile test results. The results show that the computational simulation is able

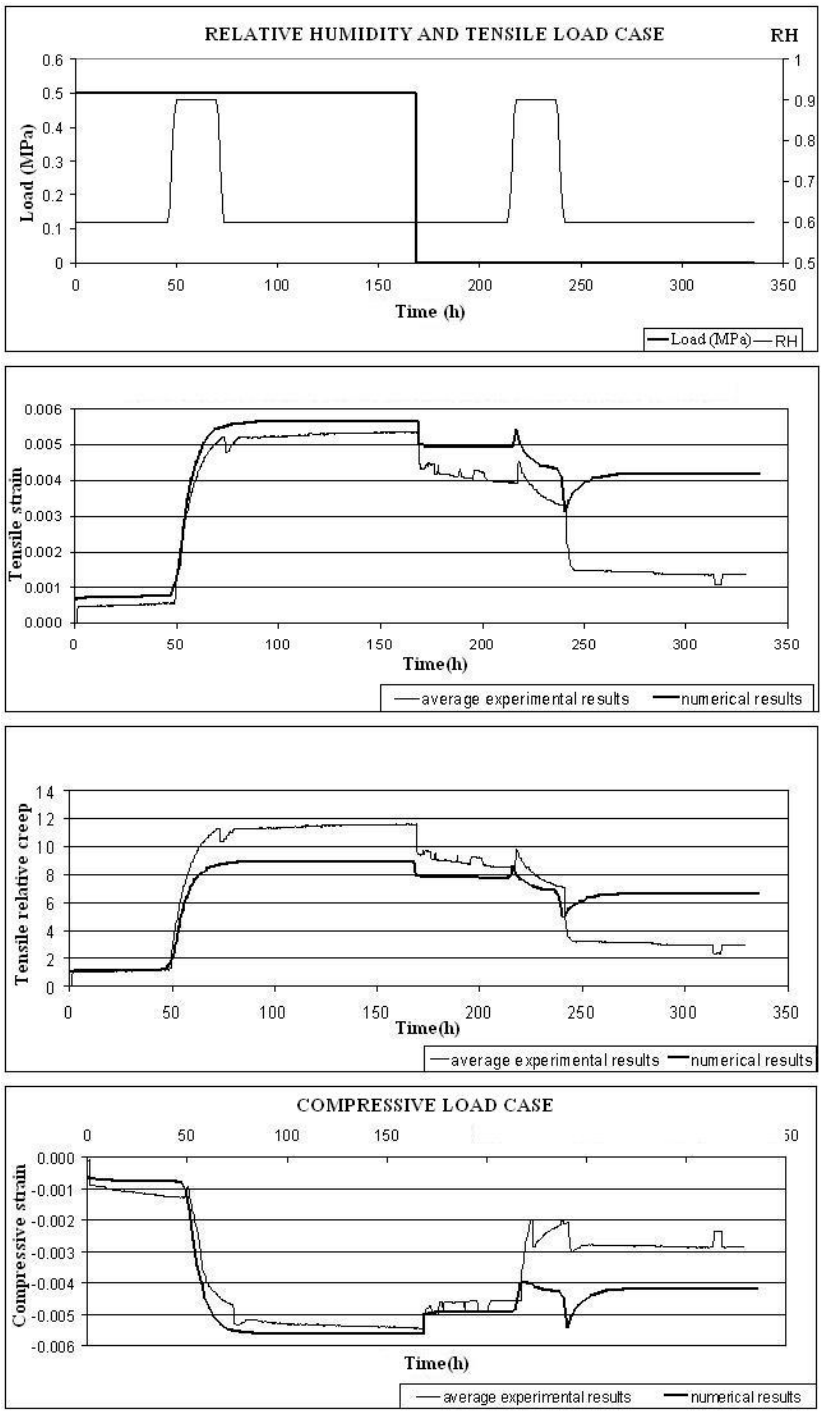

Figure 5.2: Test **?**. Short–term analysis. Tension case: mechanical loading, relative humidity, shrinkage–free strains and relative creep. Compression case: strains versus time.

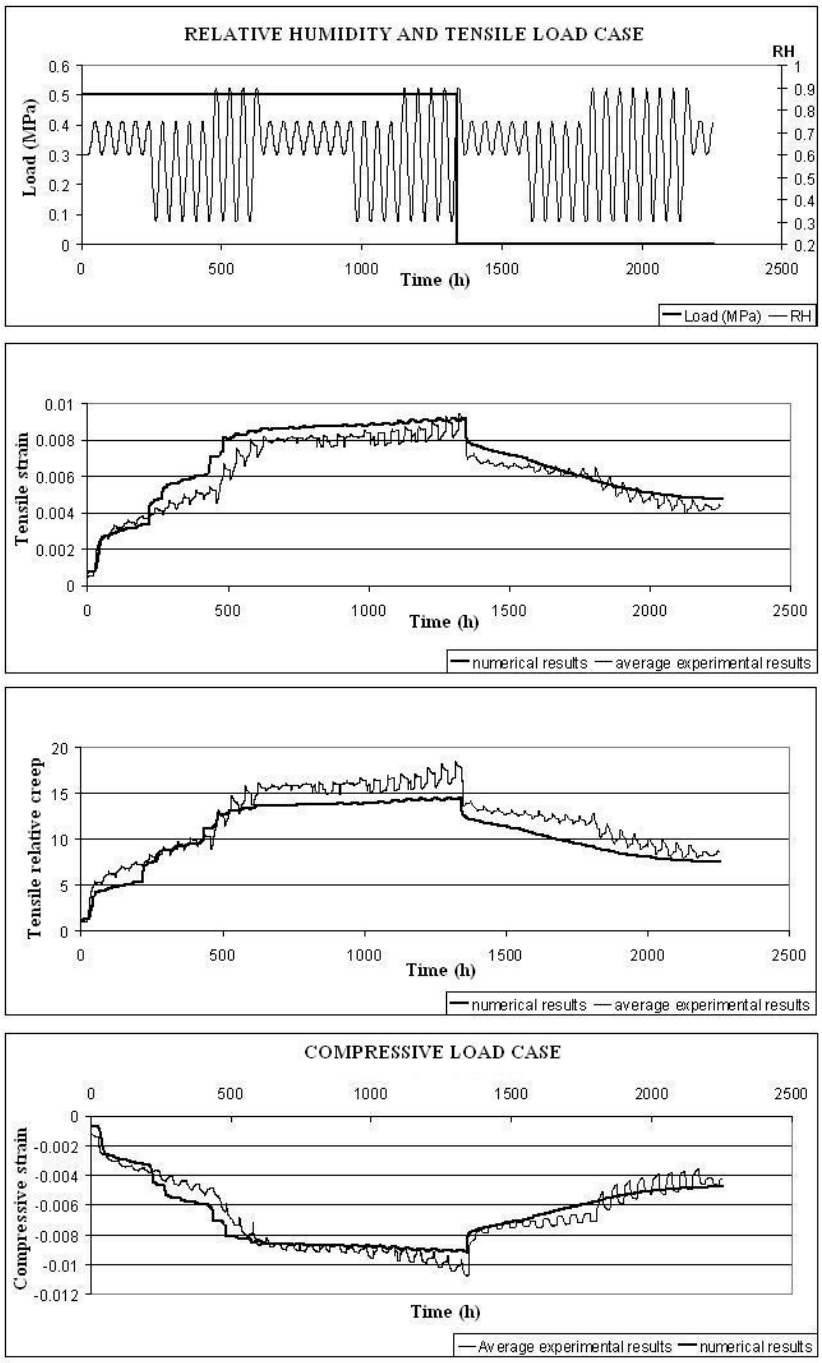

Figure 5.3: Test **?**. Long–term analysis. Tension case: mechanical loading, relative humidity, shrinkage–free strains and relative creep. Compression case: strains versus time.

to fit well these experimental data considering that the scatter of the original test results was high. Also the comparison with the experimental compressive deformations (mean value of five compressive test results) shows the good performance of the computational model. An exception is however the recovery period after a humidity cycle, in fact the model is not able to fully show the recovery noticed from the experiments.

Long–term analysis

In this case, the experiments were carried out for the same specimens described above in order to study the effect of multiple cycles. The load was applied at the beginning of the test and removed after 1400 hours. The experimental results showed that the measured mechanosorptive strain was about 10 times the elastic strain while for the single humidity cycle this was about five times the elastic strain.

The comparisons between computational and experimental results for the tensile and the compressive case are presented in Fig. 5.3. Also for this multi–cycle case, shrinkage–corrected strains and relative creep curves are plotted. The results show good performance of the computational method to simulate moisture induced deformations in timber cross sections. The oscillation of the test curves, which is not as clearly shown in the model, is probably due to differences of shrinkage strains, which is highly variable in wood by nature. Most probably not all shrinkage strains were subtracted from the test results curves.

5.2.5 Comparisons with Leivo's test results (1991)

? carried out experiments in bending of beams in spruce (*Picea abies*) loaded to a stress of 10 MPa. The member cross section was 45×95 mm^2. Initially the specimens were conditioned at RH=90% and the relative humidity was cycled between RH=35% and RH=90% at a cycle length of 70 days. The starting relative humidity was RH=90%. The experiments were carried out in a constant temperature of $T = 21°$C. The relative creep for eight specimens was measured. The values of material stiffness parameters are reported in Table 5.3.

The geometry of the beam and the Abaqus model used in the present work are shown in Fig. 5.4. To model the wood parts, 7207 elements C3D8T are used. Because of the presence of a steel plate attached to the wood beam, 2D shell elements S3 and a rigid body option are used to mesh the plate. The contacts are modeled by a hard contact pair with a penalty method in the tangential direction using a 0.4 penalty factor.

The results presented in Fig. 5.5 show that the simulated relative creep is within the scatter of the experimental relative creep curves. The computational model seems to perform well also in the grain direction.

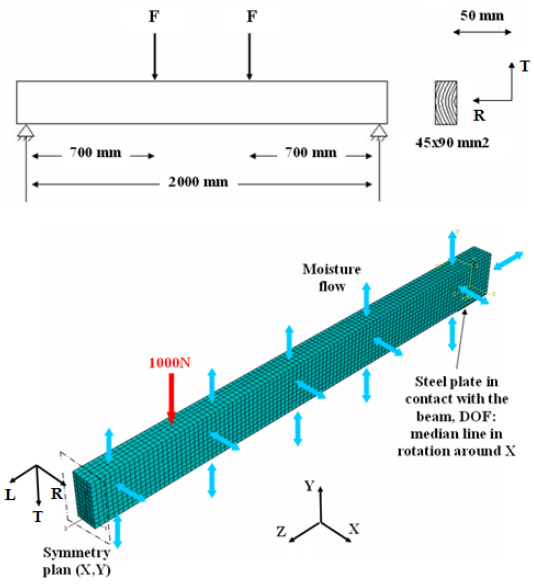

Figure 5.4: Bending test **?**. Top: geometry of the wood bending beam. Bottom: Abaqus model.

Table 5.3: Mechanical properties for Norway spruce (*Picea abies*) used in the analysis.

E_R (MPa)	E_T (MPa)	E_L (MPa)	ν_{RT}	ν_{RL}	ν_{TL}	G_{RT} (MPa)	G_{RL} (MPa)	G_{TL} (MPa)
600	600	12000	0.558	0.038	0.015	40	700	700

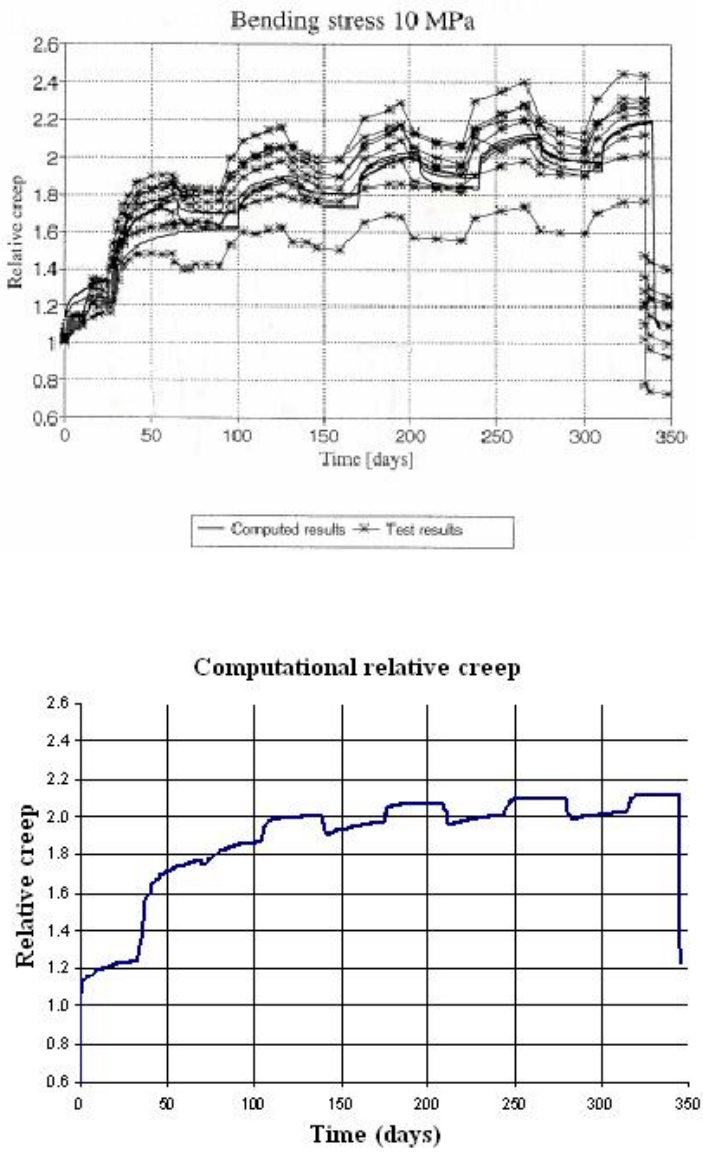

Figure 5.5: Bending test **?**. Wood bending beam. Top: experimental and computational relative creep curves from (**?**). Bottom: computational results by the computational model presented in this work.

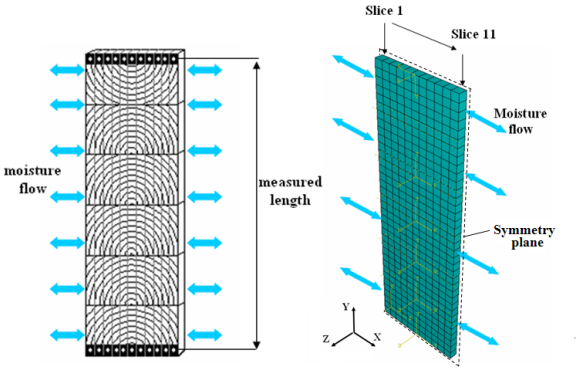

Figure 5.6: Test ?. Left: geometry of the glulam beam. Right: Abaqus model (X-Y-Z: global coordinate system).

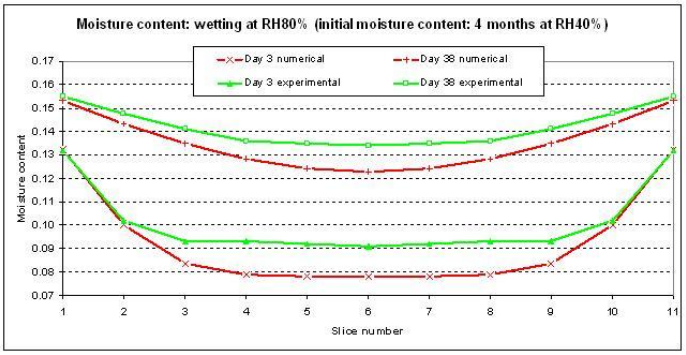

Figure 5.7: Test ?. Average of the humidity for each slice. Comparisons between computational and experimental results.

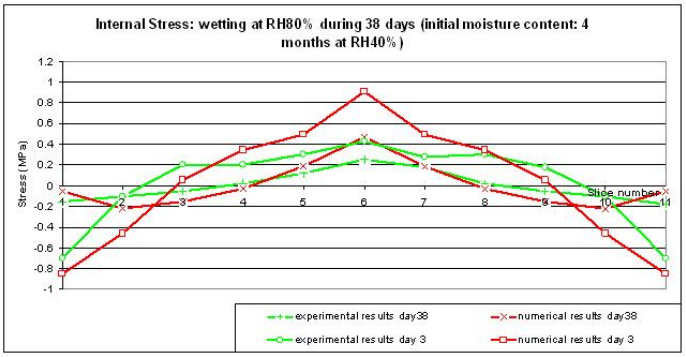

Figure 5.8: Test ?. Average of the tangential stress for each slice. Comparisons between computational stresses and experimental mean stresses.

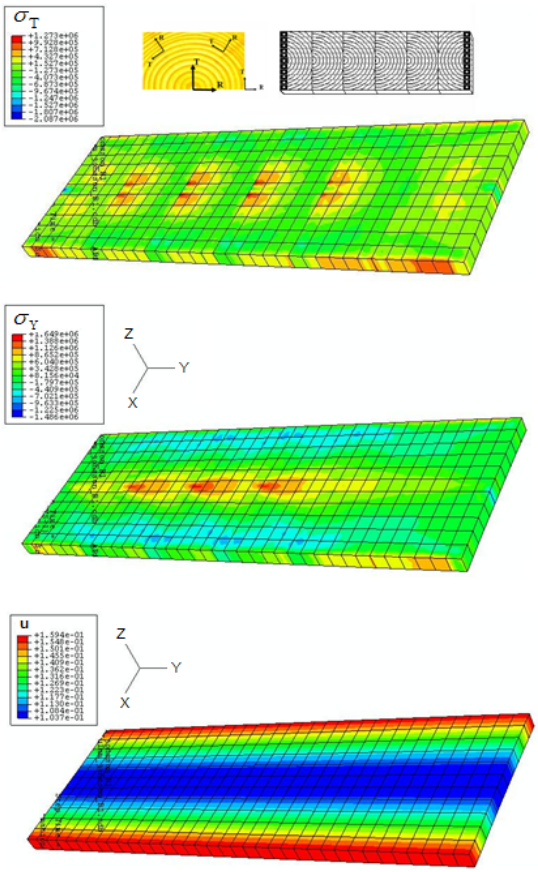

Figure 5.9: Test **?**. Analysis after 4 months and 38 days. Top: tangential stresses in material coordinates. Centre: tangential stresses in global coordinates. Bottom: Moisture content distribution.

5.2.6 Comparisons with Jönsson's test results (2005)

This comparison case is used for studying the internal stresses perpendicular to grain in glued laminated (glulam) timber beams. The described beam section was experimentally analyzed by **?**. The tested glulam beams (90×270, grade L40) contained six lamellae of Norway spruce (see properties in Table 5.3). The glulam plate specimen were subjected to an internal moisture gradient in the width direction by altering the ambient air relative humidity from the equilibrium condition of RH=40% to RH=80%. Only the two opposite sides of the specimen were open to air. At different stages, after 3 days and after 38 days of moistening, the specimens were sliced in order to measure the moisture and stress gradients in the piece. The specimen was sawn into 16 mm thick plates perpendicular to the beam axis, so that the knot free specimens had dimensions $16 \times 90 \times 270$ mm. From a single specimen, 11 slices in the width direction were sawn. The length between markers in a slice was measured before and after sawing by an optical method. The mean stress was determined from the mean released strain (ε_{mean}) for each slice:

$$\sigma_{mean} = E(u)\, \varepsilon_{mean} \tag{5.10}$$

where the elastic modulus $E(u)$, depending on the moisture content, was measured with a dynamic method.

For the numerical simulation by Abaqus, 396 quadratic elements C3D20T are used. Fig. 5.6 shows the geometry of the Jönsson glulam beam section and the model analyzed by Abaqus/Standard. The computational results in terms of moisture content (Fig. 5.7) and tangential stress (see Fig. 5.8), show a relatively good agreement with the experimental data. The distribution of stress and moisture are shown in Fig. 5.9.

Chapter 6

Results

In this chapter some of the simulations performed during the work are presented. The simulations have been useful for testing and validating the implementations. For each simulation first general considerations are reported, then input values and details are described, and finally obtained results are given.

6.1 Moisture-stress simulations

Four cases were considered for the moisture-stress simulations.

- the first is about Wadsö experiments **?**, **?**,
- the second is about Jönsson experiments **?**,
- the third is about a Lisbon bridge measurements,
- the forth is about KTH experiments.

For each simulation as preprocessing the .inp file, the user file and some files with calculations (e.g. some worksheets with Ms Excel®) we previously need for them, were prepared.

For each simulation as post processing comparisons between multi Fickian, single Fickian and experimental solutions were made.

As said in 3, in this chapter you can see which values for p_{atm}, C_1, c_{21}, c_{22}, c_{23}, c_{24},C_3, C_4, f_1,f_2, f_3, v_{air}, L, $D_b^L, D_b^T, D_v^0, \xi_L, \xi_T$ have been used.

6.2 Wadsö experiments

6.2.1 Test

The test refers to **?**. It's a pure wetting process. An increment of external RH happens and moisture content increases. There is only one direction flow. The geometry is the one in figure **??**.

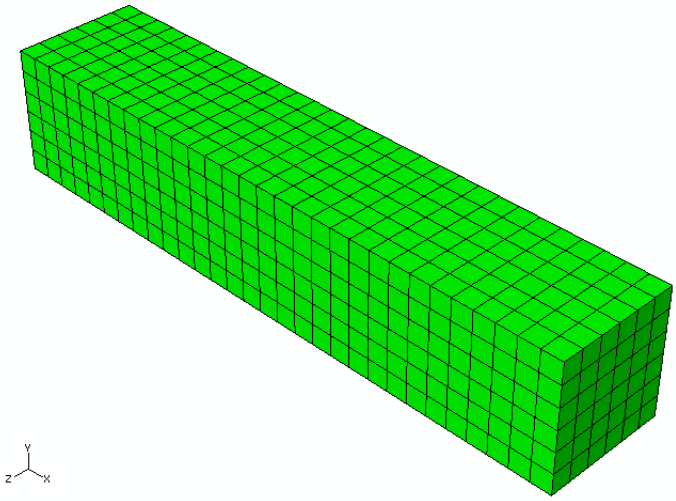

6.2.2 Input

$$\mathbf{D_b} = 7e-6m^2/s\exp\left(\frac{-E_b}{RT}\right)$$

$$\mathbf{D_v} = 0.03\left(2.31\times10^{-5}\left(\frac{p_{atm}}{p_{atm}+p_v}\left(\frac{T}{273K}\right)^{1.81}\right)\right)m^2s^{-1}$$

f_1	f_2	f_3
2.22	15.7	-14

Table 6.1: Shape parameters of the isotherm calibrated to the measurements on at C **?**

C_1 (s^{-1})	C_3	C_4 (s^{-1})
2.6e-6	50	8e-8

Table 6.2: Shape parameters of the H_c function

c_{21}	c_{22}
5.21e-6	19.0

Table 6.3: Shape parameters of C_2

6.3 Jönsson

6.3.1 Test

The test refers to **?**. It's a pure wetting process. An increment of external RH happens, moisture content increased. There is only one direction flow. The geometry is the one in figure **??**.

6.3.2 Input

Jonsson beam is a parallelepiped and it has an height of, a width of and a thickness of Geometry

The mesh used consists of [number] elements.

Initial values of $h = 0.40$ and $m = 0.12$.

The simulation time is that of the RH history.

There are only Neumann boudary conditions on two opposite faces, so we have a one direction flow

Wood and surrounding ambient properties

The material used in the simulations is the same. It's spruce.

The used values of dry wood density, wood porosity and surrounding conditions are reported into table 6.3.2. As atmospheric pressure value, the standard one $p_{atm} = 101325Pa$ has been used. Whereas as saturated vapor pressure has been calculated a value according to equation 3.34.

dry wood density	ρ_0	450.0 kg/m3
porosity	φ	0.65
atmospheric pressure	p_{atm}	101325 Pa
saturated vapor pressure	p_s	2344.025 Pa
temperature	T	293.15 K

Table 6.4: Wood and surrounding ambient properties

Sorption isotherm

The sorption isotherm used for the Jönsson simulation is given in the figure **??**. The coefficients of the curve have been obtained by curve fitting.

The following values as shape parameter of the isotherm have been used. These values have been referred by Frandsen in **?** at page 32.

f_1	f_2	f_3
0.528889	13.98889	-10.5

Table 6.5: Shape parameters of the isotherm calibrated to the measurements on at C **?**

Diffusivity values

In the simulations the following values of diffusivity coefficients were used.

$$\mathbf{D_b} = D_b^0 \exp\left(\frac{-E_b}{RT}\right) \tag{6.1}$$

$$\mathbf{D_v} = \xi 2.31 \times 10^{-5} m^2 s^{-1} \left(\frac{p_{atm}}{p_{atm} + p_v}\left(\frac{T}{273K}\right)^{1.81}\right) \tag{6.2}$$

Jonsson .

xi = 0.1285, secondo analisi parametrica D_b^0 = 3e-11 m2/s, Frandsen's report

Wadso, Frandsen .

xi = 0.03, D_b^0 = 7e-6 m2/s, Frandsen Thesis

Diffusion coefficient values used are the following:

$$\begin{bmatrix} D_b^L & 0.0 \\ 0.0 & D_b^T \end{bmatrix} = \begin{bmatrix} 7 & 0.0 \\ 0.0 & 17.5 \end{bmatrix} \times 10^{-6} m^2 s^{-1} \tag{6.3}$$

$$\begin{bmatrix} \xi_L & 0.0 \\ 0.0 & \xi_T \end{bmatrix} = \begin{bmatrix} 0.9 & 0.0 \\ 0.0 & 0.03 \end{bmatrix} \tag{6.4}$$

$$D_v^0 = 2.31 \times 10^{-5} m^2 s^{-1} \tag{6.5}$$

Here are the diffusivity coefficients.

Sorption rate

The following values as shape parameter of the H_c have been used. These values have been referred by Frandsen in **?** at page 36. Equation 3.23 has been used for calculating C_2.

h	D_v

Table 6.6:

m	D_b
0.0	0.0

Table 6.7:

6.3.3 Results

MC solution on a path at midheight at different time points has been plotted and compared with single Fickian solution and experimental values.

Experimental values are available at time points 3072 hours and 3912 hours.

Paramenters have been calculated by fitting muli Fickian solution to experimental data.

6.4 Lisbon Bridge

6.4.1 Test

The test should reproduce the behaviour of a a glulam beam of a glulam pedestrian bridge, Parque das Nações, Lisbon, Portugal. Experimental data by Lina Nunes and Pedro Palma from LNEC, project EU-INTERREG "MEDACHS"

- The moisture content values are based on measurements of electric resistance of wood by a sensor/logger "Scanntronik Materialfox Mini"
- the electrodes are stainless steel screws
- bridge erected in 2006; measured values since 17.01.2007 to 11.09.2007

6.4.2 Results

Solution has been compared with single Fickian and experimental results. Numerical results by Tononi, Usardi et al. (single-Fickian) and Mendicino et al. (multi-Fickian), 2010.
The period for the analysis reaches 11208 hours (from 01.06.2006 to 11.09.2007)

6.5 KTH

6.5.1 Test

In the project work by KTH, proton NMR imaging was applied for recording the moisture distribution of various wood specimens. The main objective was to

C_1 (s^{-1})	C_3	C_4 (s^{-1})
3.8e-4	80	1e-5

Table 6.8: Shape parameters of the H_c function

c_{21}	c_{22}	c_{23}	c_{24}
3.579	2.21	1.591e-3	14.98

Table 6.9: Shape parameters of C_2

monitor spatially resolved moisture kinetics upon changing relative humidity of the air. Wood samples of Norway Spruce (Picea abies) were used in this study. Cylindrical pieces of ca 6 mm in diameter and 20 mm long were cut from the same larger wood material. Sample axes were parallel to the main tree axes, denoted R, T, or L, where L corresponds to the longitudinal direction, R to the radial direction across the annual rings and T to the direction tangential to the annual rings. The samples were first equilibrated at 65% relative humidity (RH) over NaNO2 saturated solution. Reaching the steady-state moisture content (MC) was verified by gravimetric measurements.

Samples:

- Uncoated, T, L, R orientations
- Aquatop coated, T and R orientations
- Oil coated (Linogurad), T and R
- Adhesive bond samples (MUF adhesive), T and R
- Uncoated sample of 58 mm long cylinder, mixed orientation

6.5.2 Results

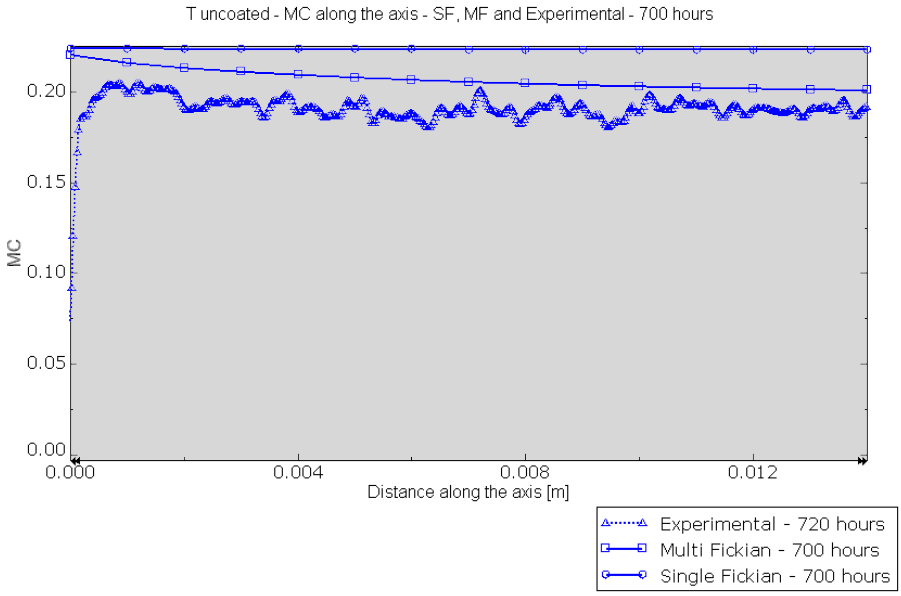

Figure 6.1: T unco 700h

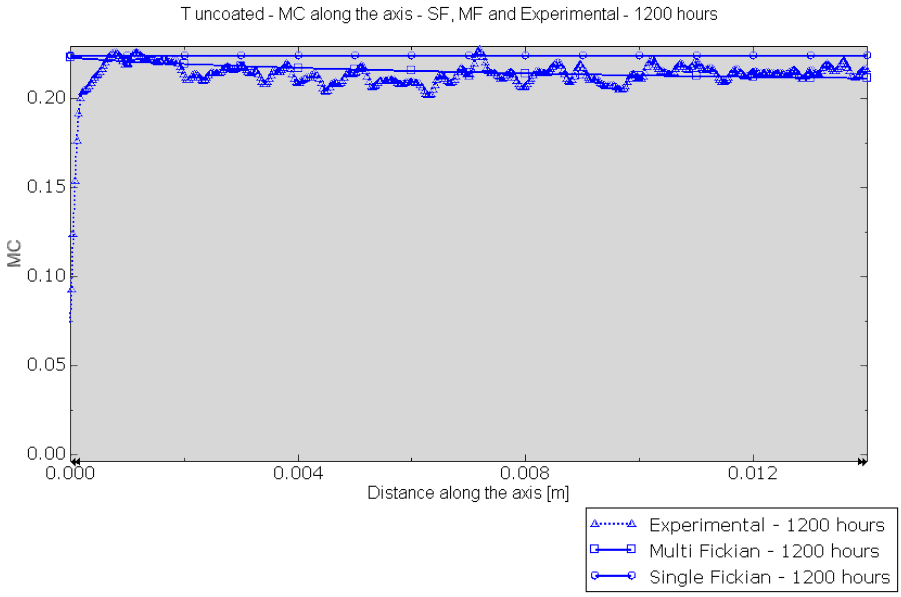

Figure 6.2: T unco 1200h

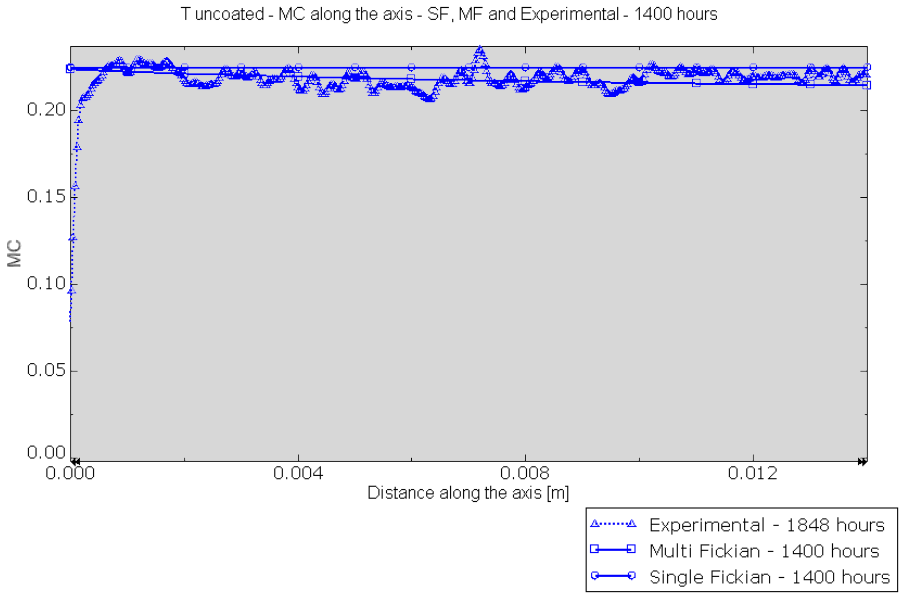

Figure 6.3: T unco 1400h

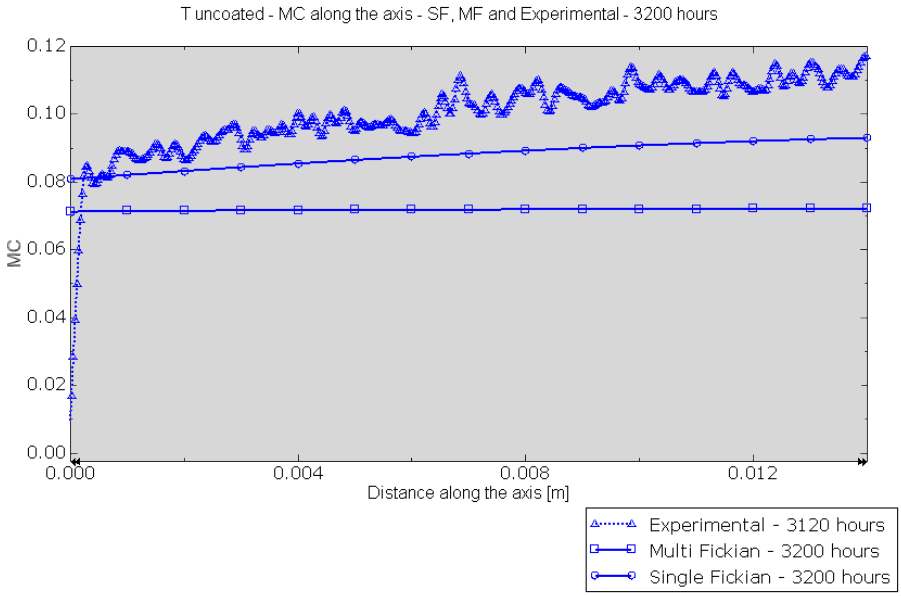

Figure 6.4: T unco 3200h

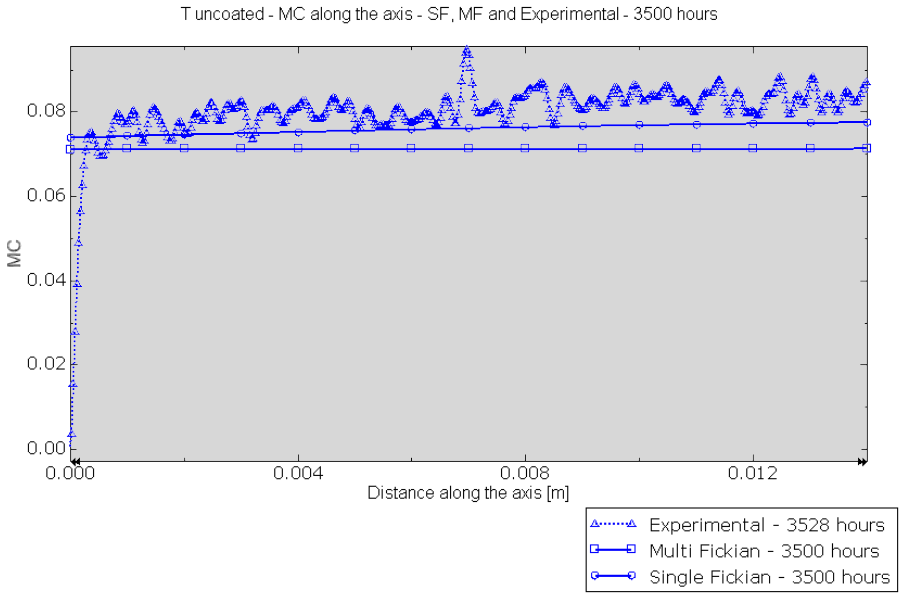

Figure 6.5: T unco 3500h

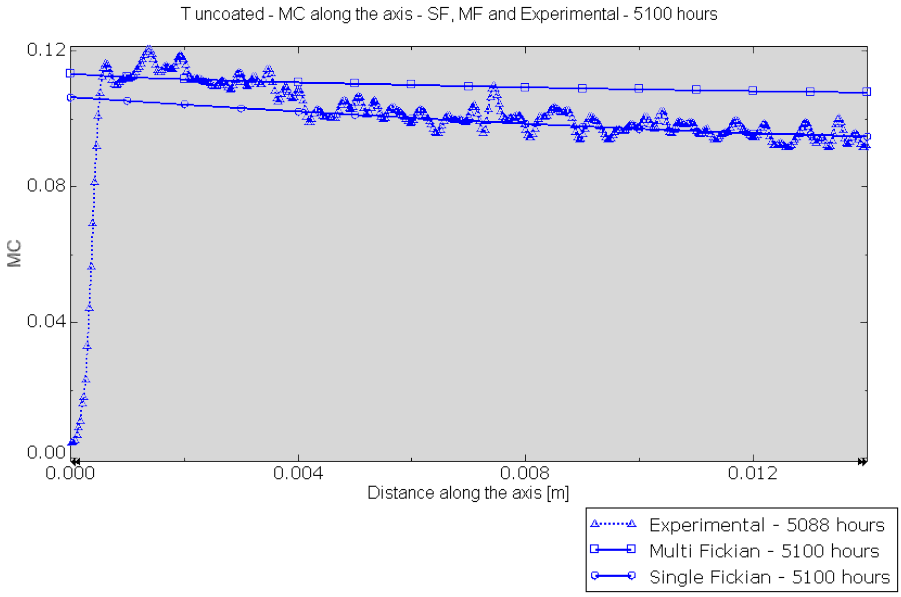

Figure 6.6: T unco 5100h

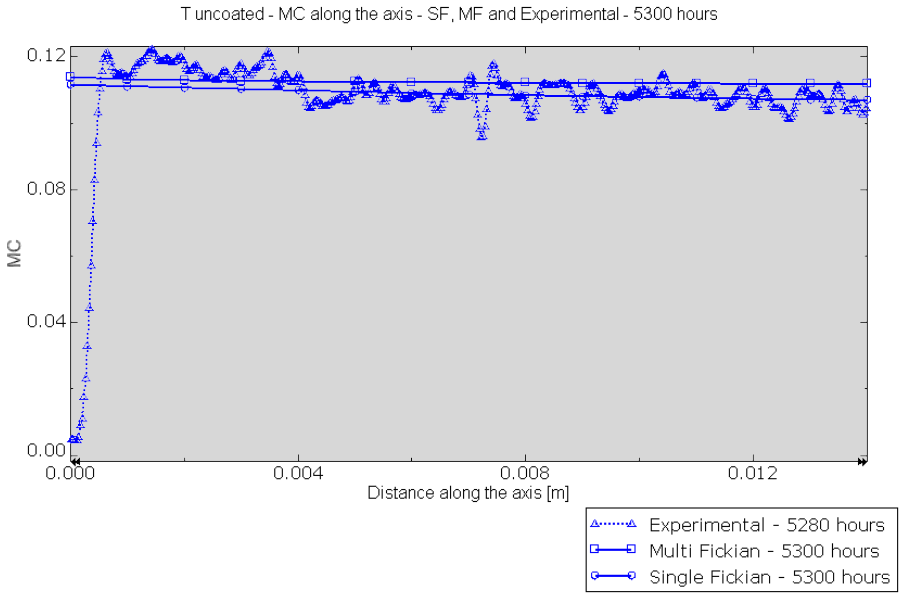

Figure 6.7: T unco 5300h

6.6 Short term Fracture simulations

A parameter analysis has been performed to calibrate our model of mDCB to some experimental results, that is to get some parameter values useful to reproduce experimental results by that numerical model.

We have considered 2 different cases, each one with a different glue in the model. The glues considered are:

- HB PU 09 or PU 09
- MUF 07

Experimental results provided by Maximillian Henningan are presented in tables 6.12 and 6.11.

Fracture toughness has been calculated according to the following formula:

$$K_{Ic} = \frac{F}{B\sqrt{W}} f$$

Fracture energy has been calculated according to the following formula:

$$G_f = \frac{I}{B(W-a)}$$

Specimen	MUF 07	HBPU 09
Width B [m]	0.00453	0.00473
W[m]	0.12	0.12
Load F [N]	126.88	145.81
Factor f	2.82	2.82
Fracture toughness K_{Ic} [kN/m$^{\frac{3}{2}}$]	228.09	251.04

Table 6.10: Experimental Results - Fracture Toughness

Specimen	MUF 07	HBPU 09
Width B [m]	0.00453	0.00473
Length of notch a [m]	0.01	0.01
W[m]	0.12	0.12
Crack length $W - a$ [m]	0.11	0.11
Integral (I) [N mm]	179.50	199.17
Fracture energy G_f [Nm/m^2]	360.22	382.80

Table 6.11: Experimental Results - Fracture energy

The integral I has been calculated as

$$I = \sum_{i=2..n} \frac{F_i + F_{i-1}}{2}(u_i - u_{i-1})$$

where $(F_i, u_i), i = 1..n$ are the experimental points and stroke measure has been used as displacement.

Specimen	MUF 07	HBPU 09
W[m]	0.12	0.12
Length of notch a [m]	0.01	0.01
$a/(W + a)$	0.69	0.68
Max. crack opening [mm]	1.95	2.08

Table 6.12: Experimental Results - other results

In the numerical model which has been calibrated we used values presented in tables 6.13, 6.14.

A damage initiation criterion of max stress and a displacement-based damage evolution criterion with exponential softening were used in the fe model.

The Glue material parameters varying in the parametric analysis are:

- T_{max}, maximum traction, after that damage starts,

E_R	900	MPa
E_T	600	MPa
E_L	12000	MPa
ν_{RT}	0.558	
ν_{RL}	0.038	
ν_{TL}	0.015	
G_{RT}	40	MPa
G_{RZ}	700	MPa
G_{TL}	700	MPa

Table 6.13: Wood Constitutive parameters

$E_L[MPa]$	longitudinal Young modulus for PU 09 glue	26500
$E_L[MPa]$	longitudinal Young modulus for MUF 07 glue	16500
$E_T[MPa]$	transverse Young modulus for both glues	10

Table 6.14: Cohesive elements elastic parameter values

- u_{max}, maximum displacement, after that the element doesn't contribute anymore to stiffness,
- α, exponent of damage exponential law

$T_{max}[Pa]$	2.15e6	2.2e6	2.25e6
$u_{max}[m]$	0.8e-4	1.2e-4	1.6e-4
$\alpha[-]$	0.6	1.0	1.4

Table 6.15: Parameter values used in the parametric analysis of the PU 09 glue

Among the curves calculated by the parametric analysis performed a best one has been chosen on the basis of a least squares measure. In particular the one which is given by the following criterion

$$\min_i \sqrt{\sum_j \left(\bar{x}_j - x^i(t_j)\right)^2}, i = 1..n, j = 1..m \tag{6.6}$$

is assumed as the best one.

- n is the number of analyses performed
- m is the number of experimental values
- $\bar{x}_j$ is the generic experimental value

$T_{max}[Pa]$	1.75e6	1.7875e6	1.825e6
$u_{max}[m]$	8e-6	4.4e-5	8e-5
$\alpha[-]$	0.8	1.6	2.4

Table 6.16: Parameter values used in the parametric analysis of the MUF07 glue

- $x^i(t_j)$ is the value obtained by the i-th analysis in the generic point t_j

$x^i(t_j)$ is valued in the point t_j by the linear interpolation of the results of the i-th analysis.

	$T_{max}[Pa]$	$u_{max}[m]$	$\alpha[-]$
MUF07 c16	1750000.0	8.0e-005	1.6
PU09 c13	2150000.0	0.00012	1.0

Table 6.17: Damage Parameter values of the best fitting analyses

Using a definition of G_f as the area under the non linear part of the load-displacement curve, or following Van Der Put, half this area, the calibration of the numerical model to the experimental load-displacement curve, imply that numerical model and experimental results give the same G_f.

Specimen	MUF 07	HBPU 09
Area under non linear part of load-external sensor measure curve [N mm]	71.55	121.88
Area under non linear part of load-stroke curve [N mm]	141.37	164.74

Table 6.18: Numerical Results - Integral calculus of non linear part of load-displacemnts curves

Chapter 7

Conclusion

- A numerical method for the evaluation of moisture induced stresses in wood is used for the analysis of glulam beams showing mechanosorptive effets
- The method was previously presented in (Fortino 2009) by using a single-Fickian approach for moisture transfer model and now has been enriched by using a multi- Fickian approach.
- The numerical values of moisture content and stresses are found to be in better agreement with the experimental data with respect to the ones obtained by the single–Fickian approach. This is promising for the development and the extension of the method to more general cases of timber connections under natural humidity conditions. However, the whole method becomes computationally more expensive.
- For more general cases, the use of a multi–Fickian approach would require future computational work aimed to implement an hysteresis model suitable to describe real humidity conditions as suggested in (Frandsen2007).
- The method can be extended for the analysis of cracked timber structures
- More experimental data in different RH environments and in the presence of different coatings are needed for the validation of the moisture diffusion model

In this thesis, some tools such as a 3D orthotropic viscoelastic–mechanosorptive model for wood under variable conditions is presented.

The constitutive model is based on the 1D model for wood in longitudinal direction introduced by **?** and on the 1D model for wood in the perpendicular to grain direction proposed by **?**. For both the viscoelastic and the recoverable mechanosorptive mechanisms, Kelvin elements are used and a mechanosorptive dashpot scheme for irrecoverable mechanosorption is also taken into account.

The above creep mechanisms are added to the elastic strain and to the hygroexpansion strain. The whole model is characterized by the fact that the mechanical quantities depend on the moisture content. The temperature is considered to be constant during the studied cases. The extension of the previous 1D constitutive creep models to 3D is done by writing the problem in a thermodynamic form, as proposed by **?** for a different model used for drying and high temperatures. 3D elemental compliance matrices are defined for each element of the different creep mechanisms and an algorithm for updating the total stress is used which is a variant of the one introduced in (**?**). This computational approach is very general and can also be used for other types of materials where the creep mechanism is described by Kelvin elements.

The constitutive model and the algorithm for stress update are implemented into the UMAT subroutine of the FEM code Abaqus. The equation describing the flow across the surface is implemented into the user subroutine DFLUX. A coupled moisture–stress analysis is performed by using the analogy with the available temperature–displacement analysis of Abaqus.

The validation of the model by comparison with existing experimental data is an important part of the present paper. The computational results fit relatively well the experimental curves for both grain direction and cross grain section. However, more experimental data are needed in order to define viscoelastic and mechanosorptive compliances fully independent of the particular studied case. Modelling of strain recovery needs also further consideration. Besides small solid timber sections, the method appears also suitable for the analysis of glued laminated timber structures. The use of the presented constitutive model for the analysis of larger size timber structures, as for example connections, require some further experimental work and the comparison of the obtained experimental data with the computational results. This research topic is under development.

Both the material model and the computational method can be directly used for analyzing problems in which the effect of temperature is significant. In this case a thermal analysis and the described coupled moisture–stress analysis can be solved sequentially by using the computational tools of Abaqus. This approach will be presented by the authors in a further work.

The constitutive model and the algorithm for stress update based on elemental algorithmic operators, could be suitable for the calculation of a generalized J integral (**?**) in problems of wood fracture mechanics characterized by creep–crack growth in variable climate conditions. This research topic is under study as well.

Appendix A

Symbols

Symbols

The meaning of all the symbols used in this report is the following:

- c_b is bound-water concentration,
- $\mathbf{J_b}$ is bound-water flux,
- c_v is vapor concentration,
- $\mathbf{J_v}$ is vapor flux,
- $\dot{c}$ is sorption rate,
- p_v is vapor pression,
- φ is porosity,
- M_{H_2O} is water molar mass, $M_{H_2O} = 18.0153\text{e-}3\,\mathrm{kg/mol}$
- R is ideal gas constant, $R = 8.314\,\mathrm{J/(mol\ K)}$,
- T is temperature expressed in K,
- $\mathbf{D_b}$ is bound-water diffusivity,
- E_b is activation energy for bound-water diffusion,
- $\mathbf{D_v}$ is vapor diffusivity,
- p_{atm} is the atmospheric pressure,
- ρ_0 is dry density of wood,
- p_s is saturated vapor pressure,
- h is the relative humidity RH, $h = \frac{p_v}{p_s}$,

- m is the moisture content MC, $m = \frac{c_b}{\rho_0}$,
- c_{bl} is bound-water concentration in equilibrium with p_v,
- $\mathbf{n}$, is the operator to project fluxes onto boundary normal,
- k_p is mass transfer coefficient of the boundary layer,
- p_v^s is vapor pressure at the surface,
- p_v^a is vapor pressure in the ambient air,
- $cost(t)$ is a quantity constant in time,
- M_{da} is the molar mass of dry air, $M_{da} = 28.9644\text{e-}3\,\mathrm{kg/mol}$
- f_1, f_2, f_3 are the shape parameters for calculating sorption isotherm,
- C_1, C_2, C_3, C_4 are the shape parameters for calculating H_c function used in $\dot{c}$ calculus expression,
- $c_{21}, c_{22}, c_{23}, c_{24}$ are parameters used to calculate C_2,
- k_v is the mass convection coefficient,
- Sh is the Sherwood number,
- Re is the Reynolds number,
- L is the dimension along the flow direction,
- v_{air} is the air velocity,
- Sc is the Schimdt number,
- ρ_a is the air density,
- M_{da} is molar mass of dry air,
- μ is the viscosity,
- D_a is the air diffusivity,
- D_b^L, D_b^T are longitudinal and transversal coefficient used to calculate D_b coefficients,
- D_v^0, is the basis coefficient used to calculate D_v coefficients,
- ξ_L, ξ_T are the longitudinal and transversal reduction factors used in calculating D_v to take the hindrance of the diffusion in the cellular structure into account,
- ∇ is the gradient operator,
- $\bullet$ is the dot product operator.

Concentrations here are referred as mass per unit of dry volume. Pressure is referred as force per unit of surface. In general, it is possible to deal with moisture content and relative humidity expressed as non-dimensional fractions or as non-dimensional percentages. In the following, h and m are intended as non-dimensional fractions. It's also possible reformulate the equations substituting $m = MC(\%)/100$ and $h = RH(\%)/100$, where $MC(\%)$ and $RH(\%)$ are respectively moisture content and relative humidity expressed as non-dimensional percentages.

Appendix B

Input files listing

In the following the listing of a user file and an input file is given. The listing is not complete as in the original file but was shortened and there are some comments useful to understand the meaning of the instructions.

Acknowledgements

Part of this work has been performed at VTT, Espoo, Finland, which is gratefully acknowledged. The author would like to thank Dr. Tomi Toratti from VTT, Espoo, Finland and Henrik Lund Frandsen for the precious suggestions given.